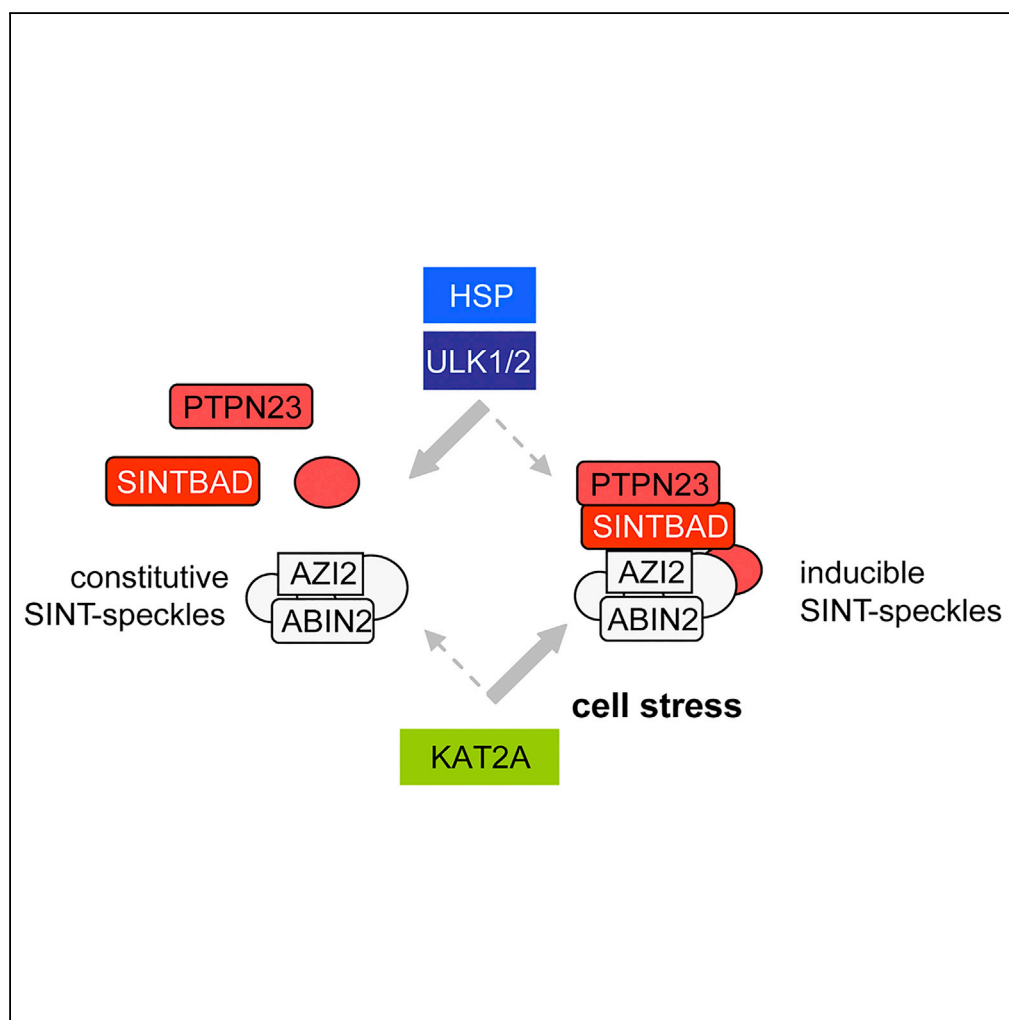


Article

ULK1/2 Restricts the Formation of Inducible SINT-Speckles, Membraneless Organelles Controlling the Threshold of TBK1 Activation



Vera Vivian Saul,
Markus Seibert,
Marcus Krüger,
Sylvia Jeratsch,
Michael Kracht,
Michael Lienhard
Schmitz

lienhard.schmitz@biochemie.
med.uni-giessen.de

HIGHLIGHTS

The SINTBAD interactors
constitute a
membraneless organelle,
the SINT-speckle

SINT-speckles are
composed of constitutive
and inducible
components

SINT-speckle formation is
controlled by ULK1,
KAT2A, and chaperone
activity

Components of SINT-
speckles control the
threshold of TBK1
activation

Saul et al., iScience 19, 527–
544
September 27, 2019 © 2019
The Authors.
[https://doi.org/10.1016/
j.isci.2019.08.001](https://doi.org/10.1016/j.isci.2019.08.001)

Article

ULK1/2 Restricts the Formation of Inducible SINT-Speckles, Membraneless Organelles Controlling the Threshold of TBK1 Activation

Vera Vivian Saul,¹ Markus Seibert,¹ Marcus Krüger,^{2,3} Sylvia Jeratsch,⁴ Michael Kracht,⁵ and Michael Lienhard Schmitz^{1,6,*}

SUMMARY

Membraneless organelles (MLOs) are liquid-like subcellular compartments providing spatiotemporal control to biological processes. This study reveals that cellular stress leads to the incorporation of the adaptor protein SINTBAD (TBKBP1) into membraneless, cytosolic speckles. Determination of the interactome identified >100 proteins forming constitutive and stress-inducible members of an MLO that we termed SINT-speckles. SINT-speckles partially colocalize with activated TBK1, and deletion of SINTBAD and the SINT-speckle component AZI2 leads to impaired TBK1 phosphorylation. Dynamic formation of SINT-speckles is positively controlled by the acetyltransferase KAT2A (GCN5) and antagonized by heat shock protein-mediated chaperone activity. SINT-speckle formation is also inhibited by the autophagy-initiating kinases ULK1/2, and knockdown of these kinases prevented focal TBK1 phosphorylation in a pathway-specific manner. The phlebovirus-encoded non-structural protein S enhances ULK1-mediated TBK1 phosphorylation and shows a stress-induced translocation to SINT-speckles, raising the possibility that viruses can also target this signaling hub to manipulate host cell functions.

INTRODUCTION

Spatial and temporal organization of cellular signaling pathways heavily relies on compartmentalization. Structural surfaces for signal transduction can be formed by membranes, components of the cytoskeleton, membrane-surrounded organelles, or membrane-less organelles (MLOs). These MLOs occur in the cytoplasm and nucleoplasm of eukaryotic cells and have recently also been discovered in bacteria (Uversky, 2017; Brangwynne, 2013; Al-Husini et al., 2018). These liquid-like subcellular compartments are believed to be formed by phase separation (Boeynaems et al., 2018), a process that involves the spontaneous separation of a supersaturated solution into a dense and a dilute phase. The liquid-like nature of MLOs allows fusion and fission events and a dynamic exchange of components. MLOs comprise a variety of subcompartments including nucleoli, promyelocytic leukemia (PML) nuclear bodies, P bodies, and stress granules (SGs) (Boeynaems et al., 2018; Darling et al., 2018; Wheeler and Hyman, 2018). The dense phase inside MLOs contains a high concentration of proteins, which may facilitate biochemical reactions and control signaling thresholds from these very crowded environments (Boeynaems et al., 2018; Gomes and Shorter, 2018; Woodruff et al., 2017). In addition, MLOs can act as dynamic buffers for RNAs and proteins. This buffering function also serves as a passive noise filter and thus reduces the inherent randomness of chemical reactions (Saunders et al., 2012). Different MLOs have a variety of functions ranging from the expression of rRNAs and pre-assembly of ribosomes (nucleoli) to the organization of the spindle apparatus (centrosomes) and mRNA splicing (splicing speckles) (Bernardi and Pandolfi, 2007; Boulon et al., 2010; Brangwynne, 2013; Hyman et al., 2014). Aberrant forms of MLOs occur upon failure of the protein quality control system or by mutation of MLO-resident proteins, often causing age-related diseases such as amyotrophic lateral sclerosis, inclusion body myopathy, and frontotemporal dementia (Hock and Polymenidou, 2016; Malinowska et al., 2013; Ramaswami et al., 2013; Taylor et al., 2016). Furthermore, various viruses hijack MLO proteins to aid in their replication (Dhillon and Rao, 2018; Möller and Schmitz, 2003; Nakagawa et al., 2018; Reineke and Lloyd, 2013). MLOs are dynamically formed by an interplay between RNA and intrinsically disordered proteins (IDPs) that typically harbor low-sequence-complexity domains enriched in polar side chains (Arg, Gln, Glu, Ser, Lys) or structure-breaking amino acids (Gly, Pro) (Uversky and Dunker, 2010). The dynamic formation of MLOs can be regulated by post-translational modifications such as acetylation, SUMOylation, or phosphorylation (Bernardi and Pandolfi, 2007; de la Vega et al., 2011; Saito et al., 2019; Wippich et al., 2013) or by environmental cues such as changes in temperature, pH, or osmolarity (Uversky,

¹Institute of Biochemistry, Medical Faculty, Friedrichstrasse 24, Justus-Liebig-University, D-35392 Giessen, Germany, Member of the German Center for Lung Research

²Institute for Genetics, Cologne Excellence Cluster on Cellular Stress Responses in Aging-Associated Diseases (CECAD), 50931 Cologne, Germany

³Center for Molecular Medicine (CMMC), University of Cologne, 50931 Cologne, Germany

⁴Max Planck Institute for Heart and Lung Research, 61231 Bad Nauheim, Germany

⁵Rudolf-Buchheim-Institute of Pharmacology, Justus-Liebig-University, D-35392 Giessen, Germany, Member of the German Center for Lung Research

⁶Lead Contact

*Correspondence: lienhard.schmitz@biochemie.med.uni-giessen.de

<https://doi.org/10.1016/j.isci.2019.08.001>



2017). Interestingly, a small interfering RNA (siRNA) screen identified several kinases as regulators of MLO formation, including the Ser/Thr kinase TBK1 as a regulator of splicing speckles (Berchtold et al., 2018).

TBK1 has been initially identified as a component of the antiviral response based on its ability to phosphorylate and thus activate IRF3 or IRF7 transcription factors, which in turn leads to inducible expression of type I interferons (IFN) (Fitzgerald et al., 2003; Sharma et al., 2003). TBK1, IRF3, and further components for induced type I IFN signaling are known to translocate to perinuclear punctate structures (Saitoh et al., 2009; Seo et al., 2016). Recent years have witnessed the identification of many additional TBK1 functions, which range from regulation of mitotic microtubule dynamics to the regulation of tumor necrosis factor-induced cell death (Lafont et al., 2018; Pillai et al., 2015; Xu et al., 2018). Furthermore, stress-regulated TBK1 functions comprise its role in autophagy, mitophagy, and xenophagy (Heo et al., 2015; Pilli et al., 2012; Wild et al., 2011). More recent evidence shows that TBK1 directly inhibits the AMP-activated protein kinase to increase energy storage and to repress respiration in adipose tissue, thus mediating a cross talk between immune signaling and metabolism (Zhao et al., 2018). Basal TBK1 signaling is also required for the development of KRAS-driven cancers (Barbie et al., 2009). Given the involvement of TBK1 in so many stress signaling pathways, TBK1 is a frequent target of viral proteins affecting its localization or protein-protein interactions (Liu et al., 2018; Onorati et al., 2016).

How can one single kinase such as TBK1 contribute to so many different signaling pathways? One possible answer to this conundrum might rely on the differential association of TBK1 to various adapter proteins, which co-determine its function (Goncalves et al., 2011). These adapter proteins include SINTBAD (TBKBP1), TANK (I-TRAF), and AZI2 (NAP1) and serve to assist in substrate binding and also affect the subcellular localization of TBK1 (Helgason et al., 2013). Although the adapter proteins lack any intrinsic enzymatic activity, they can affect biological functions, as exemplified by AZI2- and SINTBAD-regulated intracellular xenophagy of *Salmonella* (Thurston et al., 2009). SINTBAD also facilitates activation of the autophagy-initiating kinase ULK1 to control interleukin (IL)-15-induced autophagy in natural killer T cells (Zhu et al., 2018).

Here we have studied the intracellular distribution of SINTBAD and found its stress-regulated incorporation into cytosolic speckles not corresponding to the known MLO members that were tested. Determination of the SINTBAD interactome allowed the identification of proteins contained in constitutive and inducible SINT-speckles or as regulators of this dynamic process. The formation of inducible SINT-speckles is inhibited by the constitutive chaperone activity of heat shock proteins (HSPs) and ULK1 signaling, whereas KAT2A (also referred to as GCN5) promotes SINT-speckle formation. The SINT-speckle components AZI2 and SINTBAD determine the threshold of TBK1 activation, which partially occurs within SINT-speckles. Knockdown of ULK1/2 was sufficient to trigger SINT-speckle formation, but interfered with focal TBK1 activation in a pathway-specific fashion.

RESULTS

Cell Stress Triggers the Formation of SINTBAD-Containing Speckles

Many proteins participating in the induction of innate immune response signaling have a propensity to form inducible polymers or filaments, which show a reduced solubility in standard lysis buffers (David et al., 2018; Pellegrini et al., 2018; Vajjhala et al., 2017). To test the possible impact of cellular stress on the solubility of SINTBAD, HeLa cells were exposed to heat shock for different periods, followed by fractionation into a cytosolic and a nuclear/insoluble fraction representing not only chromatin proteins but also poorly soluble or aggregated proteins. A western blot analysis revealed that treatment with heat shock triggered the time-dependent transition of SINTBAD from the soluble to the nuclear/insoluble fraction, whereas this dynamic redistribution between the fractions did not occur for the SINTBAD-related proteins AZI2 or TANK (Figure 1A). A similar inducible redistribution of SINTBAD also occurred in arsenite-treated 293T cells (Figure 1B), showing that various stressors can trigger the relocation of SINTBAD in different cell types. It was also interesting to test whether SINTBAD translocation to the insoluble fraction is also seen in response to further different stimuli representing inflammatory conditions or osmotic or proteotoxic stress. These results show that most adverse agents, with the exception of inflammatory stimuli, triggered translocation of SINTBAD to the nuclear/insoluble fraction (Figure 1C). This behavior was seen for the endogenous proteins and also for the adapter proteins when expressed at moderate levels (Figures S1A and S1B).

To test whether the regulated solubility change of SINTBAD is associated with alterations of its intracellular distribution, immunofluorescence studies were performed in U2OS cells that are ideally suited and widely

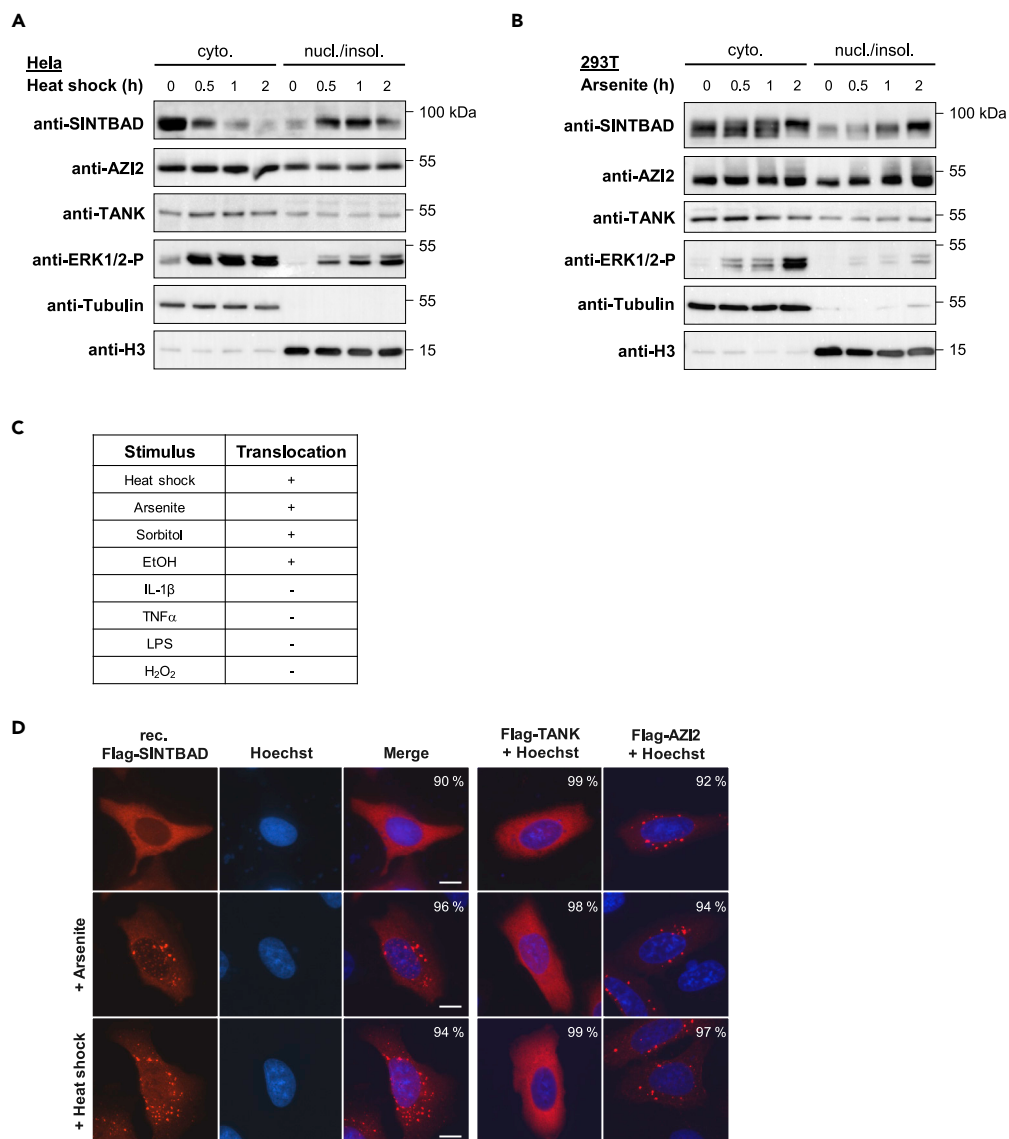


Figure 1. Stress-Inducible Formation of SINTBAD-Containing Speckles

(A) HeLa cells were exposed for the indicated periods to heat shock, and cells were harvested and fractionated into cytosolic (cyto.) and nuclear/insoluble (nucl./insol.) extracts. Western blot was performed to detect the dynamic relocalization of the endogenous adapter proteins SINTBAD, AZI2, and TANK. The detection of phosphorylated ERK1/2 (T202/Y204), tubulin, and histone H3 serves as a control for the treatment, cytosolic, and nuclear/insoluble fraction, respectively. The positions of molecular weight markers are indicated.

(B) 293T cells were treated with 0.5 mM arsenite for the indicated times and further analyzed as in (A).

(C) Different cell lines were treated with various stressors; the exact conditions are indicated in the [Transparent Methods](#) section. Following these stimulations, cells were fractionated into cytosolic and nuclear/insoluble extracts, followed by the analysis of SINTBAD translocation as described in (A and B). The occurrence of SINTBAD translocation to the nuclear/insoluble fraction is indicated by a +.

(D) Double-deficient (sgAZI2/sgSINTBAD) U2OS cells stably expressing FLAG-SINTBAD or transfected to express moderate amounts of FLAG-AZI2 or FLAG-TANK were treated with arsenite (0.5 mM, 1 h) or heat shock (43°C, 1 h) and analyzed by indirect immunofluorescence using anti-FLAG antibodies. Nuclear DNA was stained with Hoechst; scale bars, 10 μ m. The percentage of cells showing a localization as displayed in the figure is indicated.

used for the characterization of subcellular compartmentation. In the absence of a commercial antibody faithfully detecting the endogenous SINTBAD protein in immunofluorescence studies, we generated SINTBAD-deficient U2OS cells by CRISPR/Cas9-mediated genome editing ([Figures S2A and S2B](#)) that were

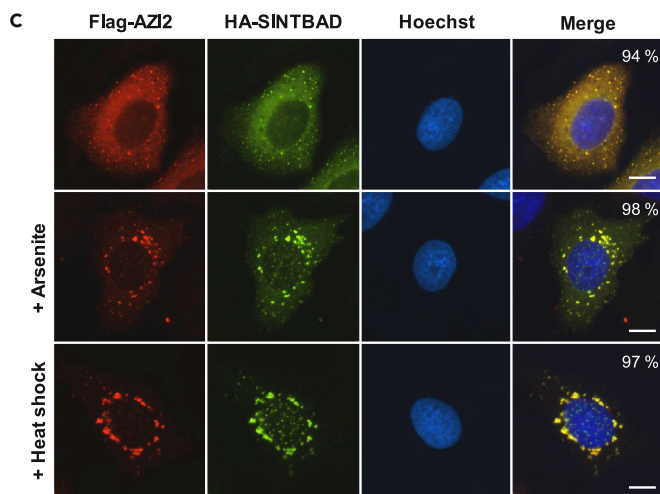
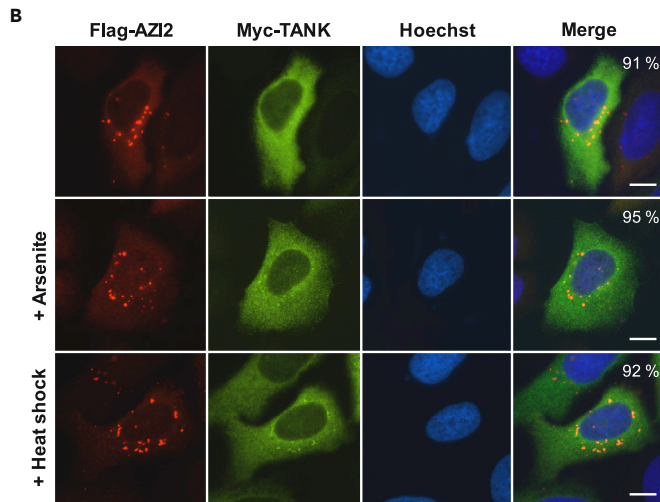
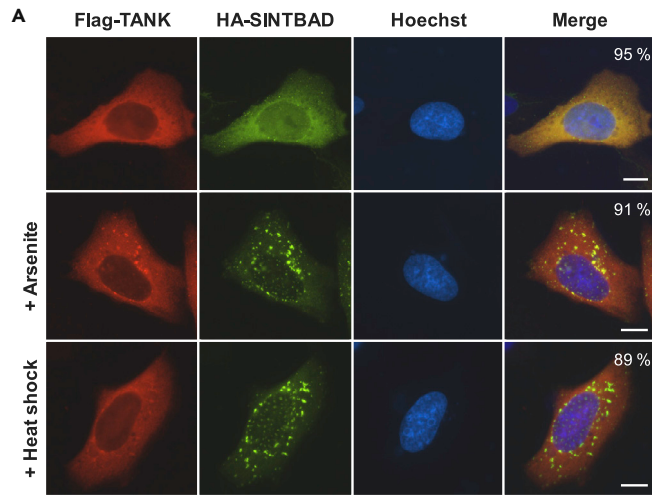


Figure 2. Comparative Analysis of TBK1 Adapter Protein Localization in Control and Stress-Exposed Cells

(A–C) U2OS cells were transfected to express moderate amounts of FLAG-TANK and hemagglutinin (HA)-SINTBAD (A), FLAG-AZI2 and Myc-TANK (B), or FLAG-AZI2 and HA-SINTBAD (C) as shown. Cells remained untreated or were exposed to arsenite or heat shock and subsequently analyzed by immunofluorescence with the indicated antibodies. Representative examples are shown, nuclear DNA was stained with Hoechst. Scale bars, 10 μ m; the percentage of cells showing the displayed phenotype is indicated.

stably reconstituted to express moderate amounts of SINTBAD fused to an N-terminal FLAG tag. We created cell clones showing SINTBAD expression levels resembling the expression of the endogenous protein and showing dynamic relocation to the insoluble fraction (Figures S3A and S3B). These cells were used to investigate its distribution in cells exposed to arsenite, heat shock, sorbitol, or Earle's balanced salt solution (EBSS) starvation medium. Untreated control cells showed SINTBAD as a largely cytosolic protein, whereas the various cell stressors triggered the formation of speckles occurring mainly in the cytosol and to a minor extent in the nucleus (Figures 1D and S4), reflecting the transition of SINTBAD from the cytosolic to the nuclear/insoluble fraction. Staining of FLAG-tagged TANK did not reveal any arsenite or heat shock-induced changes of its cytosolic localization, whereas AZI2 already showed a speckled distribution in unstressed cells that was not further influenced by the indicated stressors (Figure 1D).

It was then interesting to directly compare the intracellular colocalization of the three TBK1-binding adapter proteins in unstressed and stressed cells. Cell treatment with arsenite or thermal stress triggered the formation of speckles, whereas TANK remained largely cytosolic and showed only minor colocalization with focal SINTBAD (Figure 2A). The speckled localization of AZI2 in control and stress-exposed cells showed no significant overlap with TANK (Figure 2B). Interestingly, the coexpression of AZI2 and SINTBAD triggered the formation of speckles even in unstressed cells and displayed a very high degree of colocalization within these MLOs (Figure 2C).

Speckle Formation of SINTBAD Is Antagonized by the Chaperone Activity of Heat Shock Proteins

To test the reversibility of inducible speckle formation, cells were exposed to heat shock and then further grown at 37°C to follow the fate of speckles over time. The size and number of speckles decreased in a time-dependent manner, and speckles were not detectable after 3 h of cell recovery, as revealed by fluorescence microscopy (Figure 3A) and its quantitative analysis (Figure 3B). The resolution of speckles occurred also in the absence of *de novo* protein synthesis (Figure S5A) and in the presence of different lysosome inhibitors (Figure S5B), suggesting that lysosomal degradation and autophagic processes do not significantly contribute to this process. As chaperone function prevents aberrant phase transition of SGs (Mateju et al., 2017) it was interesting to test whether well-characterized inhibitors of HSP70 (VER155008, Pifithrin- μ) or HSP90 (geldanamycin, radicicol) affect SINTBAD localization (Massey et al., 2010; Roe et al., 1999). Inhibition of HSP70 or HSP90 function resulted in the formation of speckles even in the absence of stress signals (Figure 3C), revealing the importance of continuous chaperone function for the cytosolic localization of SINTBAD. Coimmunoprecipitation experiments showed the interaction between SINTBAD and HSP70, which was impaired under thermal stress conditions (Figure 3D). The interaction between SINTBAD and HSP90 was only detectable after coexpression of TBK1 (Figure 3E), suggesting a rather indirect interaction that can be controlled by the relative abundance of the known HSP90 interactor TBK1 (Yang et al., 2006) or that the interaction is phosphorylation dependent.

SINTBAD-Containing Speckles Show No Colocalization with Cellular Organelles or Known MLOs

TBK1 and several of its interactors including optineurin and mitochondrial antiviral-signaling protein are known to be recruited to membrane-surrounded organelles such as mitochondria (Fang et al., 2017; Moore and Holzbaaur, 2016) or upon RNA virus infection to the Golgi apparatus (Pourcelot et al., 2016). Thus, we asked whether SINTBAD would be found in association with these organelles. Costaining experiments with untreated and arsenite- or heat shock-treated cells showed significant colocalization neither with mitochondria (Figure 4A) nor with Golgi, lysosomes, peroxisomes, endosomes, or endoplasmic reticulum (Figure S6). In addition, we costained speckles with marker proteins of several known MLOs. These experiments showed colocalization of speckles neither with the SG marker proteins eIF4G (Figure 4B) or Ras GTPase-activating protein-binding protein 1 (G3BP1) nor with the P body marker DCP1a (Figures S7A and S7B).

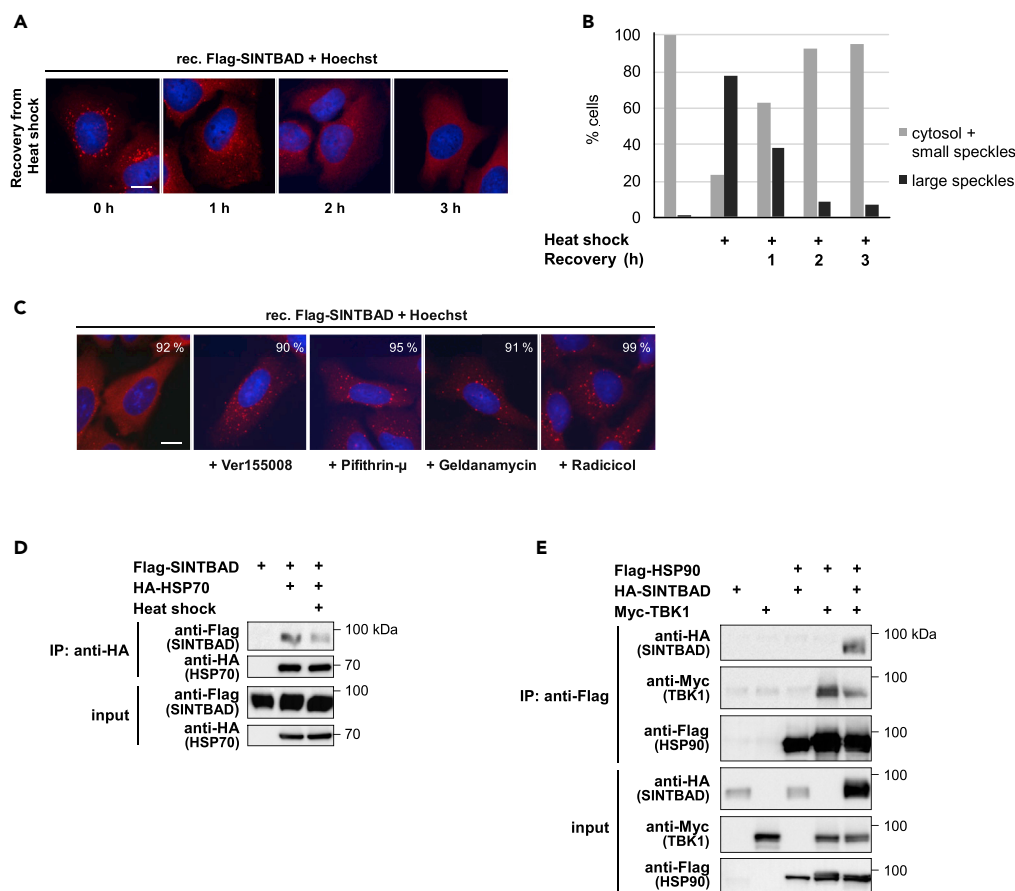


Figure 3. HSP-Mediated Chaperone Activity Is Required to Prevent SINTBAD Speckle Formation

(A) Reconstituted U2OS cells stably expressing FLAG-SINTBAD were treated with heat shock to induce speckle formation and then placed back in an incubator at 37°C for different times to allow recovery from heat shock. Speckle formation of SINTBAD was analyzed by immunofluorescence microscopy. Scale bar, 10 μ m; the percentage of cells (n = 100) showing the displayed phenotype is indicated.

(B) SINTBAD distribution in (A) was quantified by analyzing 100 cells per condition.

(C) U2OS cells stably expressing FLAG-SINTBAD were treated with the indicated chaperone inhibitors (40 μ M Ver155008, 20 μ M Pifithrin- μ , 5 μ M geldanamycin, and 1 μ M radicicol) for 2 h and then analyzed by immunofluorescence. Scale bar, 10 μ m; the percentage of cells showing the displayed phenotype is indicated.

(D) 293T cells were transfected to express FLAG-SINTBAD together with HA-HSP70. One day later, one cell dish was treated with heat shock as shown and cells were lysed. Lysates were split into two aliquots, one being used for immunoprecipitation (IP) using an anti-HA antibody. The other aliquot was used as an input control sample to ensure correct and comparable protein expression. The samples were further analyzed by western blot using appropriate antibodies as indicated.

(E) 293T cells were transfected to express FLAG-HSP90 together with HA-SINTBAD or Myc-TBK1 as shown. IP was performed using anti-FLAG antibodies, followed by western blot analysis of the IP and input samples.

Identification of SINT-Speckles

As none of these experiments related the SINTBAD-containing speckles to known subcellular structures, we aimed to identify the SINTBAD interactome by mass spectrometry. Cytosolic and nuclear/insoluble fractions were prepared from 293T cells, transfected with moderate levels of FLAG-tagged SINTBAD, followed by immunoprecipitation and identification of coprecipitating proteins by mass spectrometry as schematically shown in Figure 5A. For further bioinformatic analysis we considered proteins identified in two independent biological and technical replicates and defined high-confidence interactors by three different criteria as specified in detail in Figure S8A. This analysis revealed 150 high-confidence SINTBAD interactors of which 27% were found in the cytosol, 58% in the nuclear/insoluble fraction, and 15% in both fractions. A list of the high-confidence interactors and the complete mass spectrometry dataset is given in Table S1. To validate the interaction between SINTBAD and some of the interactors by

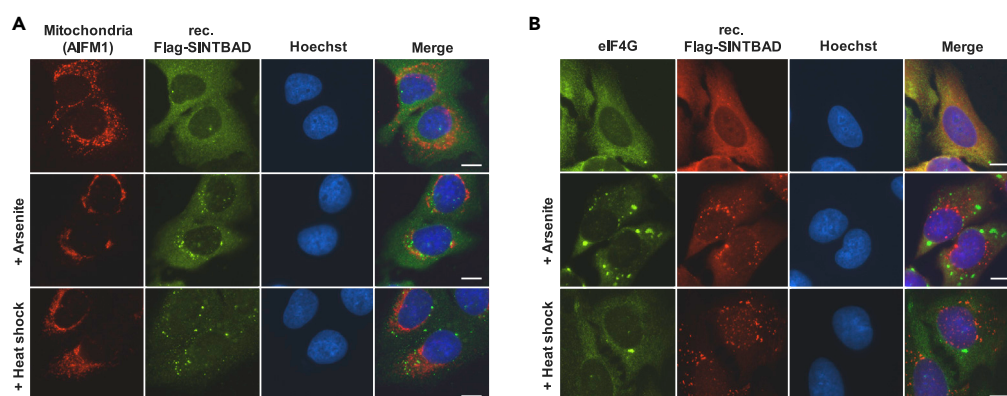


Figure 4. SINTBAD Does Not Significantly Colocalize with Membrane-Surrounded Organelles or Stress Granules

(A) U2OS cells stably expressing FLAG-SINTBAD were left untreated or exposed to arsenite or heat shock and costained with an antibody recognizing the mitochondrial marker AIFM1. A representative picture is shown. Scale bar, 10 μ m. (B) The experiments were done as in (A) with the difference that antibodies detecting the stress granule marker eIF4G were used for costaining with FLAG-SINTBAD.

an independent experimental approach we performed coimmunoprecipitation experiments. These experiments confirmed the results of the mass spectrometry analysis and are exemplified for the interaction of SINTBAD and the tyrosine phosphatase PTPN23 or the autophagy regulator AMBRA1 (Figure 5B). Also, binding of ABIN2 (A20-binding inhibitor of nuclear factor- κ B activation 2, also referred to as TNIP2) to SINTBAD was confirmed, and mapping experiments revealed the importance of the N-terminal region of SINTBAD for this interaction (Figure 5C). Interestingly, expression of SINTBAD and all of its mutants led to an increase in ABIN2 protein levels by an unknown mechanism. The other tested interactions are listed in Table S1. The identified interacting proteins are known to serve various biological functions, as displayed in Figure 5D. While the biggest group is represented by enzymes and regulators of metabolic processes, two very prominent groups represent proteins with relevance in membrane trafficking or autophagy and also mitosis and cytoskeleton dynamics. The two smallest groups are represented by regulators of innate immunity and proteins mediating transcription, probably assisting in expression of inflammatory gene expression. To test whether mutual interactions have already been described for some of the SINTBAD-interacting proteins, we analyzed the interactors in the STRING database. This analysis revealed the existence of known protein interaction networks between the 150 proteins, as visualized in Figure 5E. We then compared the intracellular localization of SINTBAD with that of some of its interacting proteins. These experiments revealed that some of the proteins such as PTPN23 exactly mirrored the behavior of SINTBAD, as shown in Figure 5F. PTPN23 localizes in the cytosol of control cells and forms speckles after induction of cell stress. Costaining with SINTBAD revealed a complete colocalization in speckles after treatment with heat shock (Figure 5F) or arsenite (Figure S8B), confirming PTPN23 as a bona fide constituent of speckles. According to the ability of SINTBAD to bind and colocalize with further proteins we term these speckles inducible SINT-speckles.

Regulation of SINT-Speckle Formation by KAT2A and ULK1/2

Further costaining experiments revealed that some interactors can trigger the formation of SINT-speckles even in unstressed cells. An example of such a positive regulator is the lysine acetyltransferase KAT2A. Expression of this predominantly nuclear protein triggered the formation of SINT-speckles even in unstressed cells and also increased the fraction of nuclear speckles (Figure 6A). Another interactor triggering the formation of SINT-speckles was ABIN2, as its expression resulted in SINT-speckle formation even in unstressed cells (Figure 6B). The dominant effect of ABIN2 also occurred for PTPN23 (Figure 6B, lower) and resembles that of AZI2, which was sufficient to trigger incorporation of SINTBAD into speckles (see Figure 2C). Accordingly, AZI2 and ABIN2 always occurred in speckles when expressed either alone (Figures 1D and 6B) or together (Figure S9). Thus, AZI2 and ABIN2 are components of constitutive SINT-speckles already occurring in unstressed cells. These proteins function as positive regulators of SINT-speckle formation, whereas expression of the already known SINTBAD interactor ULK1 (Zhao et al., 2018) revealed its

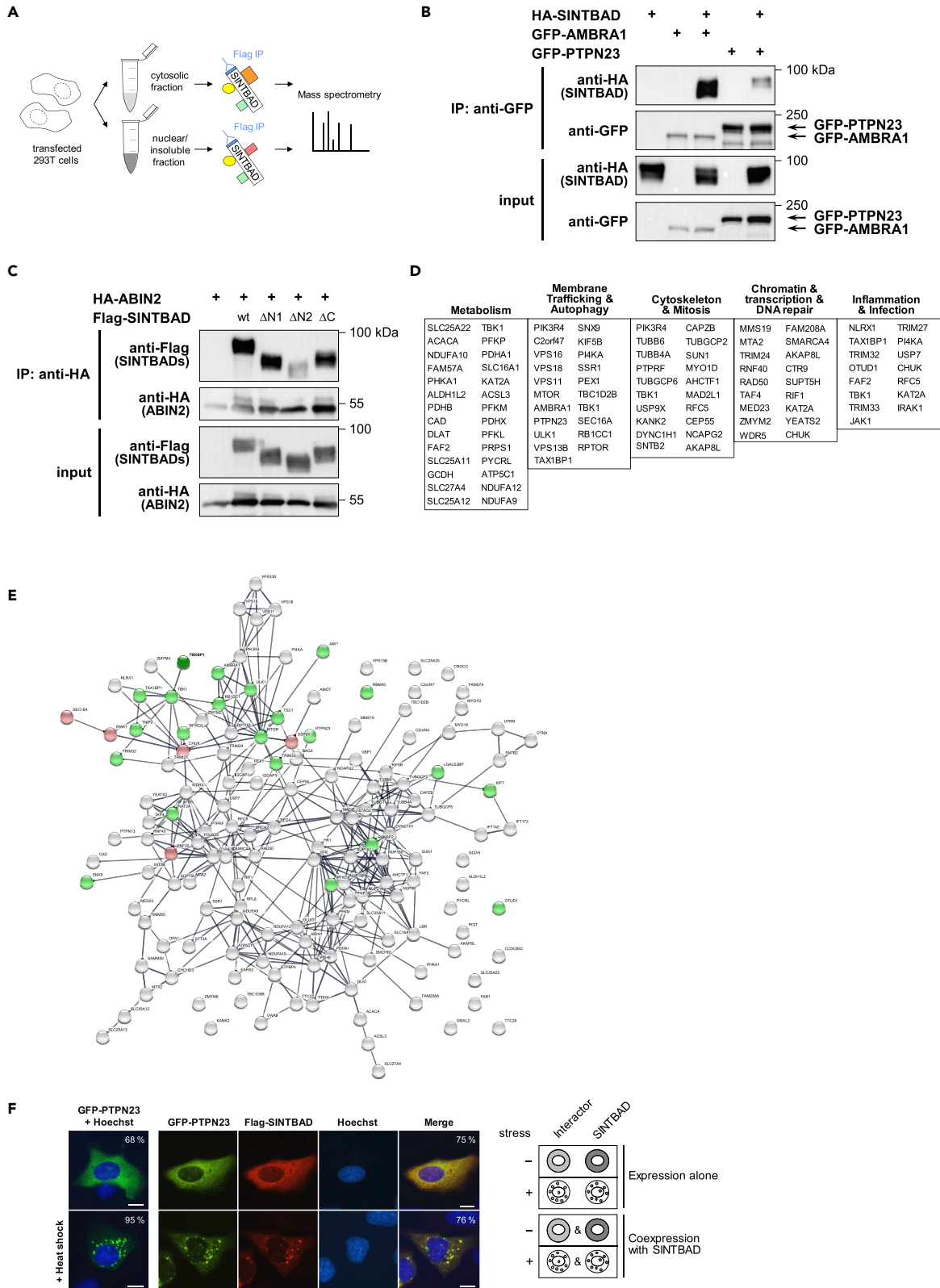


Figure 5. Characterization of the SINTBAD Interactome and Identification of SINT-Speckles

(A) Schematic display of the experimental setup used to identify SINTBAD-interacting proteins from cytosolic and nuclear/insoluble fractions. (B) 293T cells were transfected to express hemagglutinin (HA)-SINTBAD along with GFP-AMBRA1 or GFP-PTPN23. One day later, immunoprecipitation (IP) was performed using GFP-Trap beads. IP and input samples were further analyzed by western blot using appropriate antibodies as indicated. (C) An expression plasmid encoding HA-tagged ABIN2 was transfected into 293T cells together with various FLAG-SINTBAD truncation mutants (Δ N1: 106–615 amino acid [aa], Δ N2: 165–615 aa, Δ C: 1–520 aa). After IP, samples were analyzed by western blot as shown. (D) Known functions of the respective SINTBAD interactors were retrieved from databases and Pubmed searches. Proteins were assigned to the functional groups as displayed; proteins with several functions are found in more than one group. Only the five largest functional groups (>10 proteins per group) are shown. (E) Visualization of interacting protein networks in the SINTBAD interactome using the STRING database (Version 11.0). Line thickness indicates the strength of data support. SINTBAD (TBKBP1) is highlighted in dark green and written in bold. Proteins that were tested for their interaction with SINTBAD by co-IP (data not shown) are marked in green or red, indicating a confirmed or unconfirmed interaction, respectively. (F) U2OS cells were transfected to express the SINTBAD interactor PTPN23 alone and were left untreated or exposed to heat shock, followed by the analysis of GFP-PTPN23 localization by fluorescence microscopy. In addition, cells cotransfected to express GFP-PTPN23 and FLAG-SINTBAD were treated the same way. A representative experiment is shown. Scale bar, 10 μ m; the percentage of cells showing the displayed phenotype is indicated. The right part schematically summarizes the intracellular localization of the proteins.

inhibitory function for the incorporation of SINTBAD into SINT-speckles in control and heat shock- (Figure 6C) as well as in arsenite-treated cells (Figure S10). A kinase-inactive ULK1 K46I point mutant (Chan et al., 2009), in contrast to the ULK1 wild-type, formed speckles upon cellular stress when expressed alone (Figure 6D). Coexpression of the kinase-inactive mutant with SINTBAD resulted in the formation of SINT-speckles even in unstressed cells, emphasizing the importance of ULK1 kinase activity for controlling SINT-speckle formation. To determine the consequences of ULK knockdown on SINT-speckle formation we interfered with the expression of ULK1 and also ULK2, as both kinases can have redundant functions (Lee and Tournier, 2011; Li et al., 2016). Loss of both kinases already triggered the formation of SINT-speckles even in unstressed cells (Figure 6E), supporting the finding that constitutive ULK signaling is important for restriction of SINT-speckle formation. These kinase-dependent regulatory processes could enable regulation of SINT-speckle formation, as MLOs are highly dynamic and their formation is typically also regulated during the cell cycle (Rai et al., 2018). This also applies to SINT-speckles, which do not occur in unstressed or stressed mitotic cells (Figure 6F).

SINT-Speckle Components Control the Amplitude and Localization of Activated TBK1

As expression of ULK1 can trigger TBK1 phosphorylation (Zhao et al., 2018), we tested the effect of ULK1 expression on the localization of phosphorylated TBK1. ULK1-expressing cells lacked any areas with focal TBK1 phosphorylation, as the activated kinase was found in the cytosol (Figure 7A), revealing that ULK1 can control the distribution of phosphorylated TBK1. To test whether loss of ULK1 and ULK2 affects TBK1 phosphorylation in response to thermal stress, the expression of both kinases was downregulated with specific siRNAs (Figure S11). Immunofluorescence analysis of control cells revealed the heat shock-activated TBK1 in focal structures mainly in the nucleus with a partial overlap with cytosolic SINT-speckles. Downregulation of ULK1/2 largely inhibited the heat shock-induced phosphorylation of TBK1 (Figure 7B), suggesting an important contribution of these kinases for this activation pathway. In contrast, arsenite-induced TBK1 phosphorylation was not changed by ULK1/2 knockdown and occurred to a significant part in SINT-speckles (Figure 7B), showing that the ULK kinases control phosphorylation of TBK1 in a pathway-specific manner.

It was then interesting to test whether cell stress also leads to changes in the intracellular distribution of TBK1. Treatment with arsenite or heat shock resulted in a partial recruitment of TBK1 to SINT-speckles (Figure 7C), suggesting that this previously identified interaction (Ryzhakov and Randow, 2007) also occurs in MLOs. To investigate a possible contribution of SINTBAD for the activation of TBK1, SINTBAD and AZI2 double-deficient U2OS cells were treated for various periods with arsenite and TBK1 activation was assessed with a phospho-specific antibody by immunoblotting. Knockout of SINTBAD alone had no effect (data not shown), whereas cells lacking SINTBAD and AZI2 (Figure S2) showed reduced TBK1 phosphorylation (Figure 7D). To investigate the contribution of SINTBAD and AZI2 for ULK1-induced TBK1 phosphorylation by an independent experimental approach, cells were transfected to express ULK1 together with SINTBAD and/or AZI2. Immunoblotting revealed that ULK1-triggered TBK1 phosphorylation was further enhanced by SINTBAD and AZI2 (Figure 7E), corroborating the finding that both adaptor proteins contribute to control of the TBK1 activation threshold.

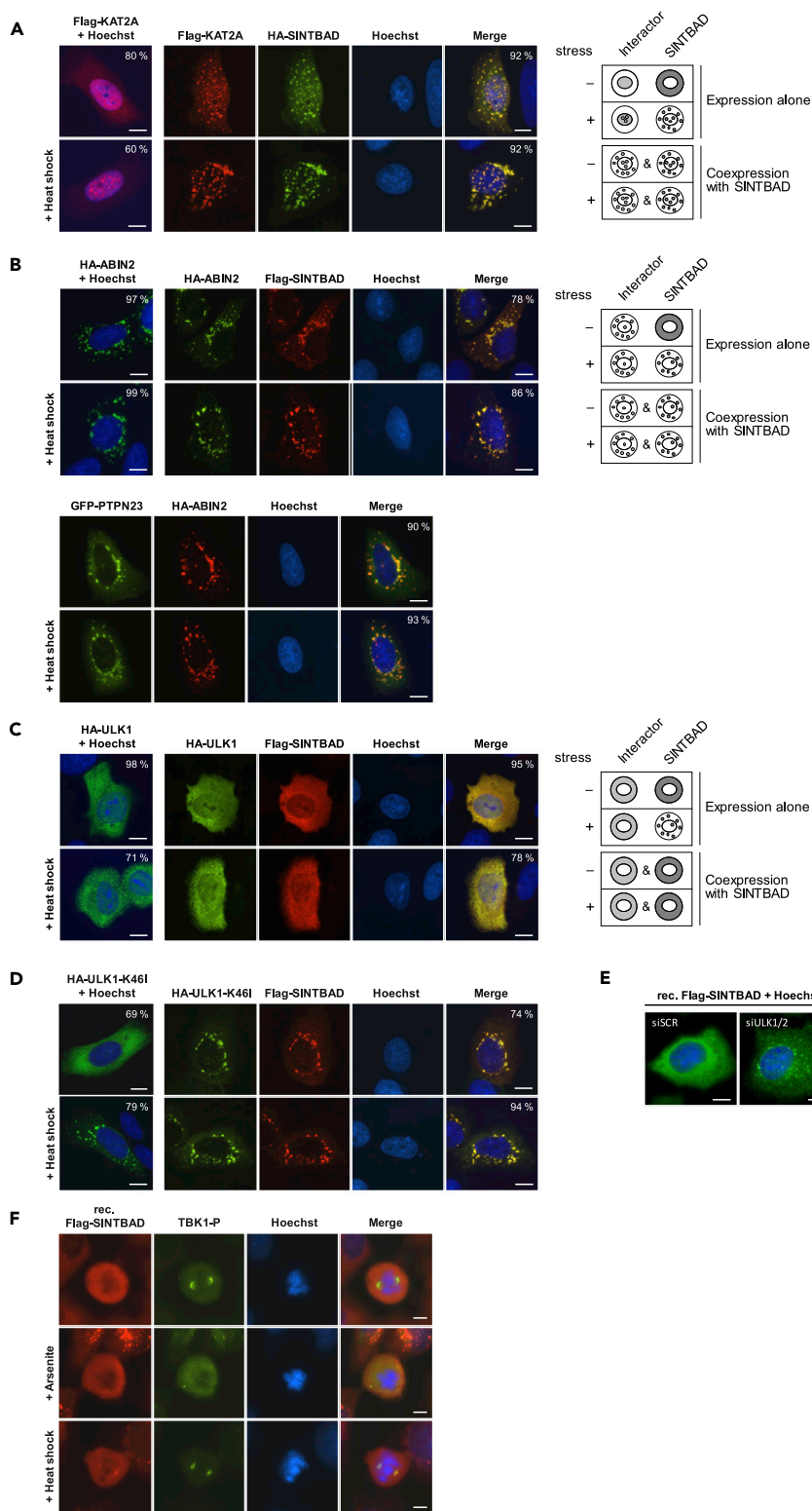


Figure 6. Characterization and Regulation of SINT-Speckles

(A) U2OS cells were transfected to express the SINTBAD interactor KAT2A alone and were left untreated or exposed to heat shock, followed by the analysis of FLAG-KAT2A localization by fluorescence microscopy. In addition, cells

Figure 6. Continued

cotransfected to express FLAG-KAT2A and hemagglutinin (HA)-SINTBAD were treated the same way. Scale bar, 10 μ m. The right part schematically summarizes the intracellular localization of the proteins.

(B) Upper: The experiment was done as in (A) with the difference that HA-ABIN2 was expressed either alone or together with FLAG-SINTBAD as shown. Lower: Cells were cotransfected to express GFP-PTPN23 and HA-ABIN2, followed by exposure to heat shock and the analysis of colocalization by immunofluorescence as shown. Scale bars, 10 μ m.

(C) U2OS cells were transfected to express HA-ULK1 alone or together with FLAG-SINTBAD. Cells were left untreated or exposed to heat shock, stained, and analyzed by fluorescence microscopy. Scale bars, 10 μ m. The right part schematically summarizes the results.

(D) The experiment was performed as in (A), except that a kinase-inactive HA-ULK1-K46I mutant was transfected into U2OS cells.

(E) Reconstituted SINTBAD-deficient U2OS cells were treated for three days with siRNAs specifically targeting ULK1 and ULK2 or alternatively with a control siRNA. Cells were then analyzed by fluorescence microscopy for the intracellular distribution of SINTBAD as shown. Scale bars, 10 μ m.

(F) Reconstituted SINTBAD-deficient U2OS cells were exposed to arsenite or heat shock, and FLAG-SINTBAD was costained with antibodies against phosphorylated TBK1 (S172) as a centrosome marker (Pillai et al., 2015). The DNA was stained with Hoechst, and only mitotic cells were analyzed. Scale bars, 5 μ m.

A Fraction of Phlebovirus Non-structural Protein S Associates with SINT-Speckles

The severe fever thrombocytopenia syndrome phlebovirus non-structural protein S (NSs) targets the ABIN2/p105 complex to activate proviral signaling cascades (Choi et al., 2019). As ABIN2 is a core component of SINT-speckles it was interesting to investigate whether the NSs protein also can be recruited to these MLOs. Immunofluorescence analysis not only confirmed the described cytosolic localization of NSs (Choi et al., 2019) but also revealed a fraction of NSs in colocalization with ABIN2 (Figure 8A). Induction of cell stress by arsenite or heat shock resulted in an increased recruitment of NSs to SINT-speckles (Figure 8A). The expression of NSs also increased UKL1-induced TBK1 phosphorylation (Figure 8B). In summary, these data show that a virus-encoded protein affecting cellular signaling pathways such as NSs can inducibly associate with SINT-speckles.

DISCUSSION**SINT-Speckles**

Here we identified the stress-induced translocation of SINTBAD to SINT-speckles, as revealed by immunofluorescence and cell fractionation experiments. These SINT-speckles form a subcellular compartment with no significant overlap to other characterized MLOs (Darling et al., 2018). SINTBAD contains two low-complexity domains containing 12.9% Gln (residues 106–346) and 27.7% Pro (residues 340–535). Core components of constitutive SINT-speckles such as ABIN2 and AZI2, and also the inducible interactor SINTBAD, are predicted to harbor long intrinsically disordered regions (Figure 9A, Table S1), which are typical for MLO-resident proteins (Elbaum-Garfinkle et al., 2015; Nott et al., 2015; Uversky and Dunker, 2010). Accordingly, about one-third of the SINT-speckle proteins (47 from 150) are predicted to have >40% disordered regions (Table S1). The mechanisms controlling the formation of constitutive SINT-speckles are not known and might involve post-translational modifications such as ULK1/2-mediated phosphorylation. Another possible mechanism could involve the bridging of two ABIN2 dimers by binding to M1-linked tri-ubiquitin chains, which might facilitate ABIN2 assembly to higher-order signaling complexes (Lin et al., 2017). Also, changes in the relative expression levels of ABIN2 speckle components affect the formation of these MLOs, explaining the abundant finding that expression of a given protein such as ABIN2 or AZI2 can affect the intracellular localization of its interactors. This behavior is characteristic for MLO formation, and accordingly, also overexpression of SG components such as TIA1 or G3BP1 is sufficient to trigger formation of SGs (Kedersha and Anderson, 2007). This implies that physiological variations in the amounts of SINT-speckle proteins can already affect speckle formation. Regulation of ABIN2 protein levels occurs in the presence of increased glucose levels or by the kinases TPL2 or IKK α / β (Chen et al., 2013; Leotoing et al., 2011; Nanda et al., 2018), and it will thus be interesting to investigate whether these situations will affect the formation of SINT-speckles. The formation of inducible SINT-speckles is regulated by several mechanisms, as schematically shown in Figure 9B. SINT-speckle formation is triggered by the acetyltransferase KAT2A. A recent study showed the relevance of acetylation of low-complexity domains for the formation of SGs (Saito et al., 2019), and it will be interesting to investigate whether the enzymatic activity of KAT2A contributes to its ability to promote inducible SINT-speckle formation. Formation of inducible SINT-speckles is antagonized by the kinase activity of its component ULK1, raising the possibility of an autoregulatory control of speckle homeostasis. Interestingly, a recent study showed that, vice versa, SINTBAD

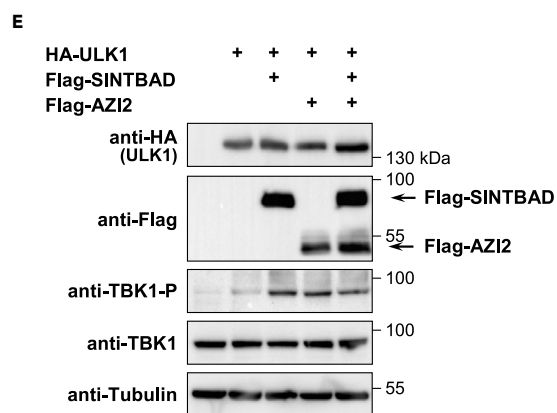
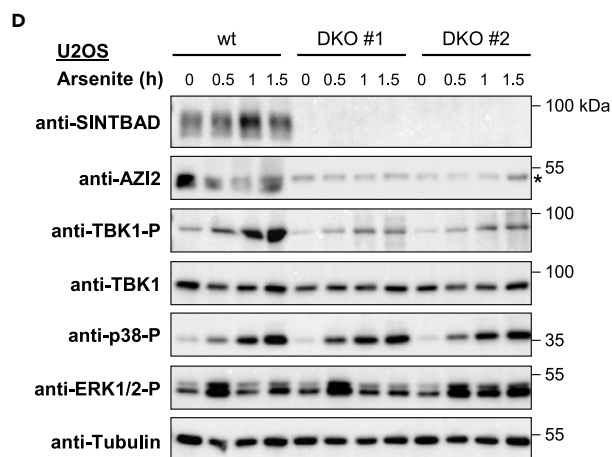
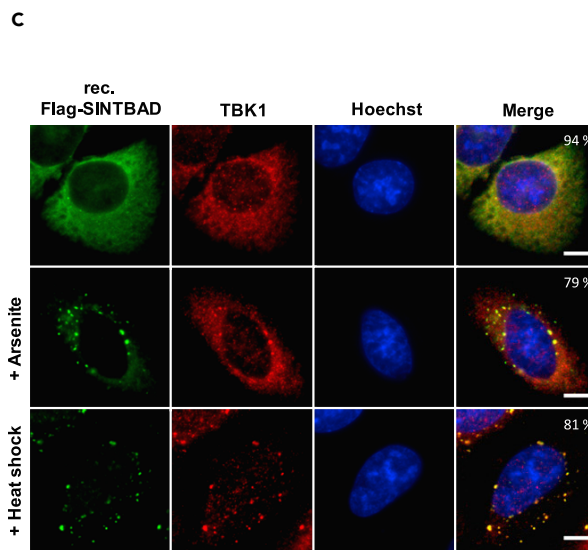
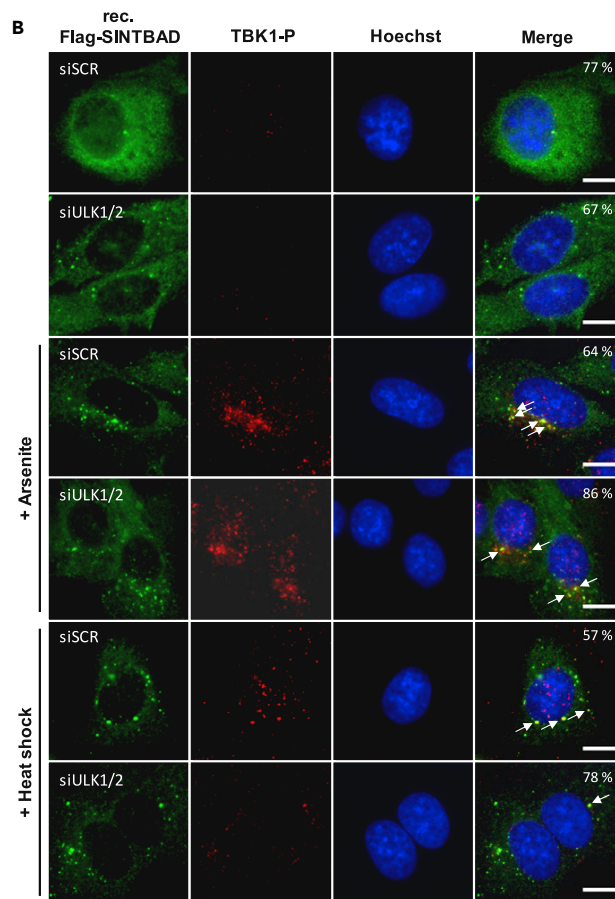
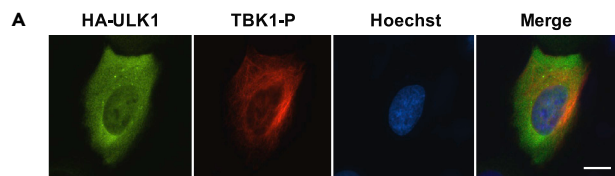


Figure 7. Regulation of TBK1 Phosphorylation by Inducible SINT-Speckles

(A) U2OS cells were transfected to express hemagglutinin (HA)-ULK1 and stained for the localization of HA-ULK1 and phosphorylated TBK1 (S172) as shown. (B) U2OS cells stably expressing FLAG-SINTBAD were treated for 3 days with siRNAs specifically targeting ULK1 and ULK2 or alternatively with a scrambled siRNA (siSCR). Cells were left untreated or exposed to arsenite or heat shock and analyzed by immunofluorescence microscopy for the intracellular distribution of SINTBAD and phosphorylated TBK1 with specific antibodies. Areas of colocalization are shown by arrows. Scale bar, 10 μ m; the percentage of cells showing the displayed phenotype is given. (C) U2OS cells stably expressing FLAG-SINTBAD were treated with arsenite or heat shock and stained for the intracellular localization of SINTBAD and TBK1 with specific antibodies. Scale bar, 10 μ m; the percentage of cells showing the displayed phenotype is given. (D) U2OS wild-type (WT) cells and two U2OS cell clones (DKO #1 and #2) lacking SINTBAD and AZI2 expression due to CRISPR/Cas9-mediated gene editing were treated for the indicated periods with 0.5 mM arsenite. Phosphorylation of TBK1 and MAP kinases (p38, ERK1/2) was determined by immunoblotting with phospho-specific antibodies as shown, to ensure successful cell stimulation. The position of a non-specific band is indicated by an asterisk. (E) 293T cells were transfected to express HA-tagged ULK1 WT along with FLAG-tagged SINTBAD or AZI2 as shown. After 1 day cell lysates were prepared and analyzed by immunoblotting for the phosphorylation of TBK1.

is required for ULK1 phosphorylation occurring during the cell type-specific induction of autophagy (Zhu et al., 2018), suggesting a mutual cross talk between these SINT-speckle components. Depletion of ULK1/2 leads to the formation of SINT-speckles in unstimulated cells. As expression of a kinase-inactive ULK1 mutant results in the spontaneous formation of SINT-speckles it is reasonable to assume an important contribution of the kinase function for this process. Also, other protein kinases function to restrict the formation of MLOs. The related kinases HIPK1 and HIPK2 decrease the size and number of PML-NBs during the cell cycle (Berchtold et al., 2018), and active DYRK3 facilitates the dissolution of several types of MLOs during mitosis (Rai et al., 2018). Kinase-dependent mechanisms might also contribute to the elimination of SINT-speckles during mitosis, a process that is accompanied by massive SINTBAD phosphorylation (Figures S12A and S12B). MLO composition can be modulated in response to stress (Boulon et al., 2010; Dellaire and Bazett-Jones, 2004), and accordingly this study reveals the recruitment of SINTBAD to SINT-speckles in response to a variety of cell stresses or after inhibition of the chaperone function of HSPs. Heat shock-induced speckle incorporation of SINTBAD can probably also be explained by the temperature-regulated SINTBAD-HSP70 interaction. The relevance of HSP70 was also shown for the prevention of aberrant SG formation (Mateju et al., 2017), and it will be interesting to reveal whether HSPs play a general role in the control of MLO integrity, as recently implicated by the analysis of the cellular chaperone network (Rizzolo et al., 2017). This study revealed the existence of a large functional chaperone supercomplex and its preferential interaction with proteins forming foci or condensates under stress conditions.

Possible Functions of Inducible SINT-Speckles

SINTBAD together with AZI2 controls the threshold of TBK1 phosphorylation, as revealed by loss-of-function and gain-of-function experiments. Active and phosphorylated TBK1 in arsenite-treated cells was largely occurring in the cytosol and showed considerable colocalization with SINT-speckles. In contrast, heat shock-induced TBK1 phosphorylation was mainly nuclear and showed only a partial overlap with SINT-speckles. These differential intracellular localizations together with their distinct dependency on upstream ULK1/2 signals suggest that several pathways lead to TBK1 phosphorylation. Thus it is conceivable that SINT-speckles serve as sites of TBK1 phosphorylation in a stimulus- and context-specific manner. The occurrence of phosphorylated TBK1 in SINT-speckles and also outside from these MLOs can be explained by the fact that only a fraction of TBK1 is found in SINT-speckles at a given time point. A further possible explanation is derived from the mechanism of TBK1 activation, where the initial activation of the kinase leads to rapid interdimer trans-autophosphorylation of its activation loop (Ma et al., 2012). This implies that after primary activation of the kinase (probably facilitated by the high local protein density in SINT-speckles) active TBK1 can rapidly spread to create high local concentrations at substrate sides. This local enrichment of phosphorylated TBK1 is frequently seen by immunofluorescence and can occur in diverse subcellular localizations (Moharir et al., 2018; Pourcelot et al., 2016). The localization of TBK1 is also controlled by differential interaction with adaptor proteins including SINTBAD, TANK, and AZI2, which compete for binding to a C-terminal interaction domain in TBK1 (Goncalves et al., 2011). Contrary to the initial assumption that the TBK1 adaptor proteins control the antiviral function of the kinase, recent publications have shown their dispensability for IRF3 activation (Fang et al., 2017).

Further possible functions of inducible SINT-speckles might be derived from a set of SINTBAD interactors, which fall into several categories (see Figure 5D). The smallest group of SINTBAD interactors comprises the expected group of innate immune regulators, but interestingly the largest group is formed by enzymes and

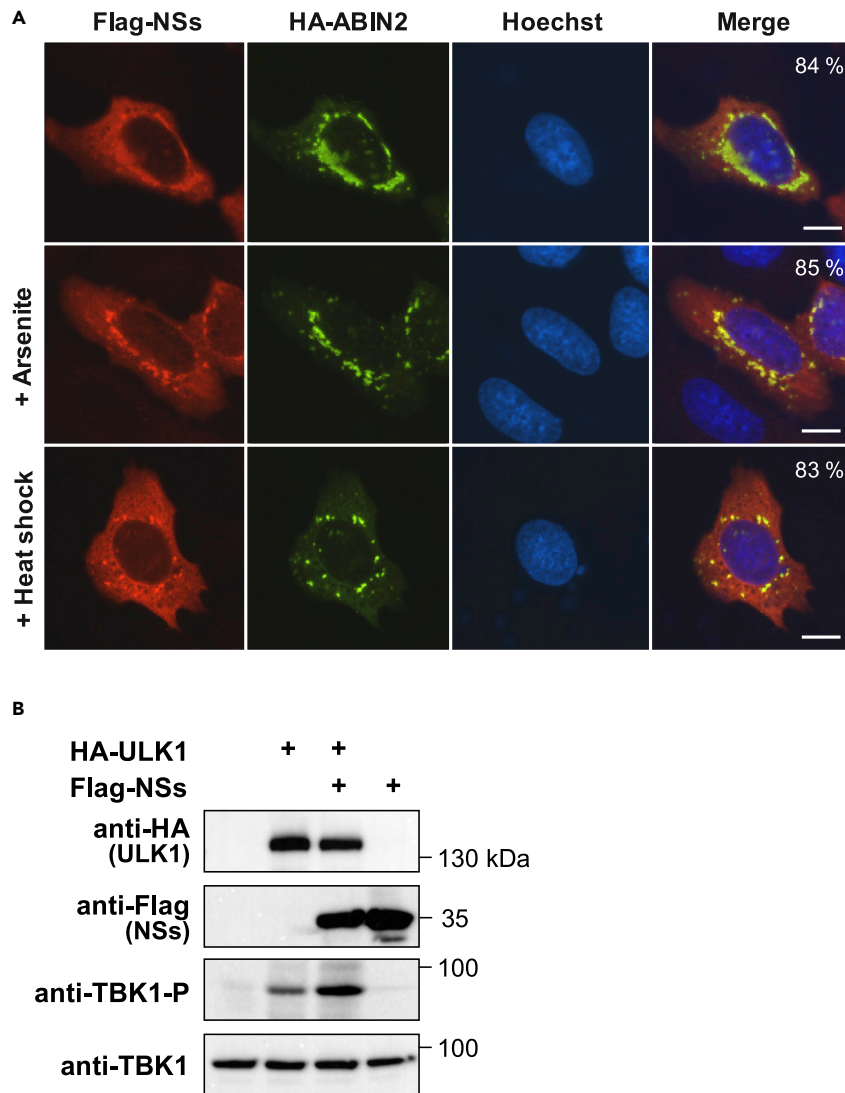


Figure 8. The Phlebovirus NSs Protein Inducibly Translocates to SINT-Speckles and Enhances ULK1-Triggered TBK1 Phosphorylation

(A) U2OS cells were transfected to express hemagglutinin (HA)-ABIN2 together with FLAG-NSs, treated with arsenite or heat shock as shown, and analyzed by indirect immunofluorescence. A representative experiment is shown; nuclear DNA was stained with Hoechst. Scale bars, 10 μ m; the percentage of cells showing the displayed phenotype is indicated.

(B) 293T cells were transfected to express HA-ULK1 and FLAG-NSs. Total cell lysates were analyzed by immunoblotting for the phosphorylation of TBK1 (S172) as shown.

regulators of cell metabolic pathways controlling glucose phosphorylation, pyruvate decarboxylation, fatty acid synthesis, and amino acid metabolism. This might indicate a role of SINT-speckles in metabolic regulation as a mediator of the cross talk between innate immunity and metabolism (Hotamisligil, 2017; Joseph et al., 2018; Jung et al., 2019). Interestingly, the ULK kinases have also been implicated in the regulation of glucose metabolic fluxes (Li et al., 2016) and lipid metabolism (Ro et al., 2013). In addition, metabolic processes co-determine effector functions and cell fate decisions of cells from the innate and adaptive immune systems (Ganeshan and Chawla, 2014; Odegaard and Chawla, 2013). Vice versa, immunomodulatory signals such as cytokines directly regulate metabolic hormones or pathways (Köchner and Brüning, 2011; Matsuki et al., 2003). The second largest group is formed by proteins involved in vesicle trafficking and autophagy, which is consistent with a previous study identifying ABIN2 as a hub protein binding to components of the endosomal sorting complex (Banks et al., 2016). This set of interactors might be also

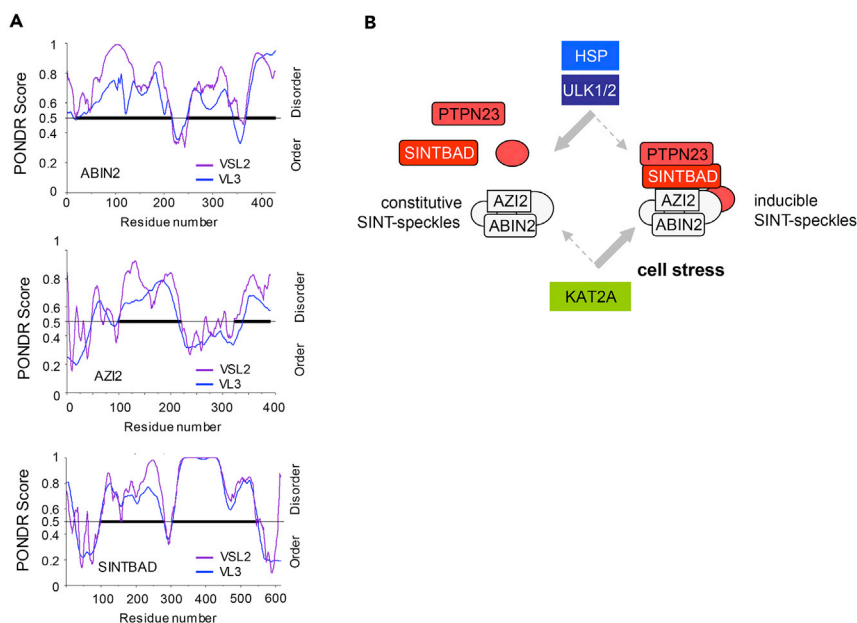


Figure 9. Potential Mechanisms Allowing Formation of SINT-Speckles

(A) The amino acid sequences of the indicated proteins were analyzed by the PONDR VSL2 and VL3 prediction tools for the identification of unstructured regions, which are highlighted by bold bars.

(B) Schematic model summarizing the regulatory events allowing assembly and disassembly of inducible SINT-speckles.

relevant for the recently uncovered role of SINTBAD as a regulator of IL-15-induced autophagy (Zhu et al., 2018), adding to the emerging role of innate immune signaling proteins such as TBK1 and TRAF6 for the formation of autophagosomes (Nazio et al., 2013; Pilli et al., 2012; Shi and Kehrl, 2010; Thurston et al., 2009). The third largest group of the SINTBAD interactome comprises regulators of mitosis and components of the cytoskeleton, in line with previous reports, documenting a function of TBK1 as a centrosome-associated regulator of mitotic microtubule dynamics (Pillai et al., 2015; Kim et al., 2013). Although this study focuses on the identification and cell biological characterization of SINT-speckles, future studies must comprehensively characterize the function(s) of constitutive and inducible SINT-speckles.

SINT-speckles might also be of pathophysiological relevance in virus infections or protein aggregation diseases. This study shows that a significant fraction of the phlebovirus NSs protein colocalize with ABIN2. It will be interesting to investigate the functional consequences of this association as well as the molecular mechanisms leading to this interaction, as the NSs protein is a structured protein (Barski et al., 2017). ABIN2 is also bound by the rabies virus-encoded M protein, which in turn controls the expression of inflammatory target genes (Besson et al., 2017), and also other components of SINT-speckles assigned to the functional group “inflammation and infection” (see Figure 5D) is targeted by viruses or involved in the antiviral response (Schmitz et al., 2014). Another possible pathophysiological scenario is due to the function of MLOs as signaling hubs in a crowded microenvironment, which can come at the cost of unwanted protein aggregation. Interestingly, partial loss of TBK1 causes protein misfolding diseases, namely, familial amyotrophic lateral sclerosis and frontotemporal dementia (Freischmidt et al., 2015; Gijssels et al., 2015). Also, mutations in TBK1 and its substrate protein optineurin contribute to frontotemporal lobar degeneration (Le Ber et al., 2015; Pottier et al., 2015). This disease is also associated with an elevated SINTBAD expression (Broce et al., 2018), and it will be very interesting to reveal in future studies whether the formation and function of SINT-speckles is affected in neurodegenerative diseases.

Limitations of the Study

In the present study we define components of constitutive and inducible SINT-speckles and reveal their regulation by ULK1/2, HSPs, and KAT2A. However, we have not identified all biological functions exerted by this dynamically regulated protein assembly.

METHODS

All methods can be found in the accompanying [Transparent Methods](#) supplemental file.

SUPPLEMENTAL INFORMATION

Supplemental Information can be found online at <https://doi.org/10.1016/j.isci.2019.08.001>.

ACKNOWLEDGMENTS

We thank Yvonne Horn, Markus Schwinn, and Georgette Stovall for excellent technical assistance. We thank the following colleagues for providing plasmids: Dr. A. Chariot (University of Liège, Belgium), Dr. B. Song (Emory University School of Medicine, Atlanta, USA), Dr. C. A. Tanase (University of Bucharest, Romania), Dr. F. Cecconi (University of Rome, Italy), Dr. R. Beyaert (VIB-Ghent University, Belgium), Dr. S. H. Tooze (The Francis Crick Institute, London, UK), Dr. Ezra Burstein (UT Southwestern, Dallas, Texas, USA), Dr. J. U. Jung (University of Southern California, Los Angeles, USA), and Dr. F. Zhang (Harvard University, Boston, USA). This work was funded by the Deutsche Forschungsgemeinschaft (DFG, German Research Foundation) - Projektnummer 109546710 - TRR81, Projektnummer 197785619 - SFB1021, and the Excellence Cluster Cardio-Pulmonary System (ECCPS, EXC 147/2).

AUTHOR CONTRIBUTIONS

V.V.S. and M.L.S. conceived the study, V.V.S., M.S., M. Krüger, and S.J. performed and evaluated experiments, M.L.S. wrote the manuscript, and M. Kracht finalized the manuscript.

DECLARATION OF INTERESTS

The authors declare no competing interests.

Received: March 25, 2019

Revised: July 8, 2019

Accepted: August 1, 2019

Published: September 27, 2019

REFERENCES

- Al-Husini, N., Tomares, D.T., Bitar, O., Childers, W.S., and Schrader, J.M. (2018). alpha-proteobacterial RNA degradosomes assemble liquid-liquid phase-separated RNP bodies. *Mol. Cell* 71, 1027–1039.
- Banks, C.A., Boanca, G., Lee, Z.T., Eubanks, C.G., Hattem, G.L., Peak, A., Weems, L.E., Conkright, J.J., Florens, L., and Washburn, M.P. (2016). TNIP2 is a hub protein in the NF-kappaB network with both protein and RNA mediated interactions. *Mol. Cell. Proteomics* 15, 3435–3449.
- Barbie, D.A., Tamayo, P., Boehm, J.S., Kim, S.Y., Moody, S.E., Dunn, I.F., Schinzel, A.C., Sandy, P., Meylan, E., Scholl, C., et al. (2009). Systematic RNA interference reveals that oncogenic KRAS-driven cancers require TBK1. *Nature* 462, 108–112.
- Barski, M., Brennan, B., Miller, O.K., Potter, J.A., Vijaykrishnan, S., Bhella, D., Naismith, J.H., Elliott, R.M., and Schwarz-Linek, U. (2017). Rift Valley fever phlebovirus NSs protein core domain structure suggests molecular basis for nuclear filaments. *Elife* 6, <https://doi.org/10.7554/eLife.29236>.
- Berchtold, D., Battich, N., and Pelkmans, L. (2018). A systems-level study reveals regulators of membrane-less organelles in human cells. *Mol. Cell* 72, 1035–1049.
- Bernardi, R., and Pandolfi, P.P. (2007). Structure, dynamics and functions of promyelocytic leukaemia nuclear bodies. *Nat. Rev. Mol. Cell Biol.* 8, 1006–1016.
- Besson, B., Sonthonnax, F., Duchateau, M., Ben, K.Y., Larrous, F., Eun, H., Hourdel, V., Matondo, M., Chamot-Rooke, J., Grailhe, R., and Bourhy, H. (2017). Regulation of NF-kappaB by the p105-ABIN2-TPL2 complex and RelAp43 during rabies virus infection. *PLoS Pathog.* 13, e1006697.
- Boeynaems, S., Alberti, S., Fawzi, N.L., Mittag, T., Polymenidou, M., Rousseau, F., Schymkowitz, J., Shorter, J., Wolozin, B., Van Den Bosch, L., et al. (2018). Protein phase separation: a new phase in cell biology. *Trends Cell Biol.* 28, 420–435.
- Boulon, S., Westman, B.J., Hutten, S., Boisvert, F.M., and Lamond, A.I. (2010). The nucleolus under stress. *Mol. Cell* 40, 216–227.
- Brangwynne, C.P. (2013). Phase transitions and size scaling of membrane-less organelles. *J. Cell Biol.* 203, 875–881.
- Broce, I., Karch, C.M., Wen, N., Fan, C.C., Wang, Y., Tan, C.H., Kouri, N., Ross, O.A., Hoglinger, G.U., Muller, U., et al. (2018). Immune-related genetic enrichment in frontotemporal dementia: an analysis of genome-wide association studies. *PLoS. Med.* 15, e1002487.
- Chan, E.Y., Longatti, A., McKnight, N.C., and Tooze, S.A. (2009). Kinase-inactivated ULK proteins inhibit autophagy via their conserved C-terminal domains using an Atg13-independent mechanism. *Mol. Cell. Biol.* 29, 157–171.
- Chen, J.Y., Chou, H.C., Chen, Y.H., and Chan, H.L. (2013). High glucose-induced proteome alterations in hepatocytes and its possible relevance to diabetic liver disease. *J. Nutr. Biochem.* 24, 1889–1910.
- Choi, Y., Park, S.J., Sun, Y., Yoo, J.S., Pudupakam, R.S., Foo, S.S., Shin, W.J., Chen, S.B., Tschlis, P.N., Lee, W.J., et al. (2019). Severe fever with thrombocytopenia syndrome phlebovirus non-structural protein activates TPL2 signalling pathway for viral immunopathogenesis. *Nat. Microbiol.* 4, 429–437.
- Darling, A.L., Liu, Y., Oldfield, C.J., and Uversky, V.N. (2018). Intrinsically disordered proteome of human membrane-less organelles. *Proteomics* 18, e1700193.
- David, L., Li, Y., Ma, J., Garner, E., Zhang, X., and Wu, H. (2018). Intrinsic mechanism of the CARMA1-BCL10-MALT1-TRAF6 signalosome. *Proc. Natl. Acad. Sci. U S A* 115, 1499–1504.
- de la Vega, L., Fröbius, K., Moreno, R., Calzado, M.A., Geng, H., and Schmitz, M.L. (2011). Control of nuclear HIPK2 localization and function by a

- SUMO interaction motif. *Biochim. Biophys. Acta* 1813, 283–297.
- Dellaire, G., and Bazett-Jones, D.P. (2004). PML nuclear bodies: dynamic sensors of DNA damage and cellular stress. *Bioessays* 26, 963–977.
- Dhillon, P., and Rao, C.D. (2018). Rotavirus induces formation of remodeled stress granules and P bodies and their sequestration in viroplasm to promote progeny virus production. *J. Virol.* 92, <https://doi.org/10.1128/JVI.01363-18>.
- Elbaum-Garfinkle, S., Kim, Y., Szczepaniak, K., Chen, C.C., Eckmann, C.R., Myong, S., and Brangwynne, C.P. (2015). The disordered P granule protein LAF-1 drives phase separation into droplets with tunable viscosity and dynamics. *Proc. Natl. Acad. Sci. U S A* 112, 7189–7194.
- Fang, R., Jiang, Q., Zhou, X., Wang, C., Guan, Y., Tao, J., Xi, J., Feng, J.M., and Jiang, Z. (2017). MAVS activates TBK1 and IKKepsilon through TRAFs in NEMO dependent and independent manner. *PLoS Pathog.* 13, e1006720.
- Fitzgerald, K.A., McWhirter, S.M., Faia, K.L., Rowe, D.C., Latz, E., Golenbock, D.T., Coyle, A.J., Liao, S.M., and Maniatis, T. (2003). IKKepsilon and TBK1 are essential components of the IRF3 signaling pathway. *Nat. Immunol.* 4, 491–496.
- Freischmidt, A., Wieland, T., Richter, B., Ruf, W., Schaeffer, V., Muller, K., Marroquin, N., Nordin, F., Hubers, A., Weydt, P., et al. (2015). Haploinsufficiency of TBK1 causes familial ALS and fronto-temporal dementia. *Nat. Neurosci.* 18, 631–636.
- Ganeshan, K., and Chawla, A. (2014). Metabolic regulation of immune responses. *Annu. Rev. Immunol.* 32, 609–634.
- Gijselsinck, I., Van, M.S., van der Zee, J., Sieben, A., Piltjens, S., Heeman, B., Engelborghs, S., Vandenbulcke, M., De, B.G., Baumer, V., et al. (2015). Loss of TBK1 is a frequent cause of frontotemporal dementia in a Belgian cohort. *Neurology* 85, 2116–2125.
- Gomes, E., and Shorter, J. (2018). The molecular language of membraneless organelles. *J. Biol. Chem.* 294, 7115–7127.
- Goncalves, A., Burckstummer, T., Dixit, E., Scheicher, R., Gorna, M.W., Karayel, E., Sugar, C., Stukalov, A., Berg, T., Kralovics, R., et al. (2011). Functional dissection of the TBK1 molecular network. *PLoS One* 6, e23971.
- Helgason, E., Phung, Q.T., and Dueber, E.C. (2013). Recent insights into the complexity of Tank-binding kinase 1 signaling networks: the emerging role of cellular localization in the activation and substrate specificity of TBK1. *FEBS Lett.* 587, 1230–1237.
- Heo, J.M., Ordureau, A., Paulo, J.A., Rinehart, J., and Harper, J.W. (2015). The PINK1-PARKIN mitochondrial ubiquitylation pathway drives a program of OPTN/NDP52 recruitment and TBK1 activation to promote mitophagy. *Mol. Cell* 60, 7–20.
- Hock, E.M., and Polymenidou, M. (2016). Prion-like propagation as a pathogenic principle in frontotemporal dementia. *J. Neurochem.* 138 (Suppl 1), 163–183.
- Hotamisligil, G.S. (2017). Foundations of immunometabolism and implications for metabolic health and disease. *Immunity* 47, 406–420.
- Hyman, A.A., Weber, C.A., and Julicher, F. (2014). Liquid-liquid phase separation in biology. *Annu. Rev. Cell Dev. Biol.* 30, 39–58.
- Joseph, A.M., Monticelli, L.A., and Sonnenberg, G.F. (2018). Metabolic regulation of innate and adaptive lymphocyte effector responses. *Immunol. Rev.* 286, 137–147.
- Jung, J., Zeng, H., and Horng, T. (2019). Metabolism as a guiding force for immunity. *Nat. Cell Biol.* 21, 85–93.
- Kedersha, N., and Anderson, P. (2007). Mammalian stress granules and processing bodies. *Methods Enzymol.* 431, 61–81.
- Kim, J.Y., Welsh, E.A., Oguz, U., Fang, B., Bai, Y., Kinose, F., Bronk, C., Remsing Rix, L.L., Beg, A.A., Rix, U., et al. (2013). Dissection of TBK1 signaling via phosphoproteomics in lung cancer cells. *Proc. Natl. Acad. Sci. U S A* 110, 12414–12419.
- Könner, A.C., and Brüning, J.C. (2011). Toll-like receptors: linking inflammation to metabolism. *Trends Endocrinol. Metab.* 22, 16–23.
- Lafont, E., Draber, P., Rieser, E., Reichert, M., Kupka, S., de, M.D., Draberoval, H., von, M.A., Bhamra, A., Henderson, S., et al. (2018). TBK1 and IKKepsilon prevent TNF-induced cell death by RIPK1 phosphorylation. *Nat. Cell Biol.* 20, 1389–1399.
- Le Ber, I., De Septenville, A., Millecamps, S., Camuzat, A., Caroppo, P., Couratier, P., Blanc, F., Lacomblez, L., Sella, F., Fleury, M.C., et al. (2015). TBK1 mutation frequencies in French frontotemporal dementia and amyotrophic lateral sclerosis cohorts. *Neurobiol. Aging* 36, 3116.
- Lee, E.J., and Tournier, C. (2011). The requirement of uncoordinated 51-like kinase 1 (ULK1) and ULK2 in the regulation of autophagy. *Autophagy* 7, 689–695.
- Leotoing, L., Chereau, F., Baron, S., Hube, F., Valencia, H.J., Bordereaux, D., Demmers, J.A., Strouboulis, J., and Baud, V. (2011). A20-binding inhibitor of nuclear factor-kappaB (NF-kappaB)-2 (ABIN-2) is an activator of inhibitor of NF-kappaB (IkappaB) kinase alpha (IKKalpha)-mediated NF-kappaB transcriptional activity. *J. Biol. Chem.* 286, 32277–32288.
- Li, T.Y., Sun, Y., Liang, Y., Liu, Q., Shi, Y., Zhang, C.S., Zhang, C., Song, L., Zhang, P., Zhang, X., et al. (2016). ULK1/2 constitute a bifurcate node controlling glucose metabolic fluxes in addition to autophagy. *Mol. Cell* 62, 359–370.
- Lin, S.M., Lin, S.C., Hong, J.Y., Su, T.W., Kuo, B.J., Chang, W.H., Tu, Y.F., and Lo, Y.C. (2017). Structural insights into linear tri-ubiquitin recognition by A20-binding inhibitor of NF-kappaB, ABIN-2. *Structure* 25, 66–78.
- Liu, X., Main, D., Ma, Y., and He, B. (2018). Herpes simplex virus 1 inhibits TANK-binding kinase 1 through formation of the Us11-Hsp90 complex. *J. Virol.* 92, <https://doi.org/10.1128/JVI.00402-18>.
- Ma, X., Helgason, E., Phung, Q.T., Quan, C.L., Iyer, R.S., Lee, M.W., Bowman, K.K., Starovasnik, M.A., and Dueber, E.C. (2012). Molecular basis of Tank-binding kinase 1 activation by transautophosphorylation. *Proc. Natl. Acad. Sci. U S A* 109, 9378–9383.
- Malinowska, L., Kroschwald, S., and Alberti, S. (2013). Protein disorder, prion propensities, and self-organizing macromolecular collectives. *Biochim. Biophys. Acta* 1834, 918–931.
- Massey, A.J., Williamson, D.S., Browne, H., Murray, J.B., Dokurno, P., Shaw, T., Macias, A.T., Daniels, Z., Geoffroy, S., Dopson, M., et al. (2010). A novel, small molecule inhibitor of Hsc70/Hsp70 potentiates Hsp90 inhibitor induced apoptosis in HCT116 colon carcinoma cells. *Cancer Chemother. Pharmacol.* 66, 535–545.
- Mateju, D., Franzmann, T.M., Patel, A., Kopach, A., Boczek, E.E., Maharana, S., Lee, H.O., Carra, S., Hyman, A.A., and Alberti, S. (2017). An aberrant phase transition of stress granules triggered by misfolded protein and prevented by chaperone function. *EMBO J.* 36, 1669–1687.
- Matsuki, T., Horai, R., Sudo, K., and Iwakura, Y. (2003). IL-1 plays an important role in lipid metabolism by regulating insulin levels under physiological conditions. *J. Exp. Med.* 198, 877–888.
- Moharir, S.C., Bansal, M., Ramachandran, G., Ramaswamy, R., Rawat, S., Raychaudhuri, S., and Swarup, G. (2018). Identification of a splice variant of optineurin which is defective in autophagy and phosphorylation. *Biochim. Biophys. Acta Mol. Cell Res.* 1865, 1526–1538.
- Möller, A., and Schmitz, M.L. (2003). Viruses as hijackers of PML nuclear bodies. *Arch. Immunol. Ther. Exp. (Warsz.)* 51, 295–300.
- Moore, A.S., and Holzbaur, E.L. (2016). Dynamic recruitment and activation of ALS-associated TBK1 with its target optineurin are required for efficient mitophagy. *Proc. Natl. Acad. Sci. U S A* 113, E3349–E3358.
- Nakagawa, K., Narayanan, K., Wada, M., and Makino, S. (2018). Inhibition of stress granule formation by middle east respiratory syndrome coronavirus 4a accessory protein facilitates viral translation, leading to efficient virus replication. *J. Virol.* 92, <https://doi.org/10.1128/JVI.00902-18>.
- Nanda, S.K., Nagamori, T., Windheim, M., Amu, S., Aviello, G., Patterson-Kane, J., Arthur, J.S.C., Ley, S.C., Fallon, P., and Cohen, P. (2018). ABIN2 function is required to suppress DSS-induced colitis by a Tpl2-independent mechanism. *J. Immunol.* 201, 3373–3382.
- Nazio, F., Strappazzo, F., Antonioli, M., Bielli, P., Cianfanelli, V., Bordin, M., Gretzmeier, C., Dengjel, J., Piacentini, M., Fimia, G.M., and Cecconi, F. (2013). mTOR inhibits autophagy by controlling ULK1 ubiquitylation, self-association and function through AMBRA1 and TRAF6. *Nat. Cell Biol.* 15, 406–416.
- Nott, T.J., Petsalaki, E., Farber, P., Jervis, D., Fussner, E., Plochowietz, A., Craggs, T.D., Bazett-Jones, D.P., Pawson, T., Forman-Kay, J.D., and Baldwin, A.J. (2015). Phase transition of a disordered nuage protein generates environmentally responsive membraneless organelles. *Mol. Cell* 57, 936–947.

- Odegaard, J.I., and Chawla, A. (2013). The immune system as a sensor of the metabolic state. *Immunity* 38, 644–654.
- Onorati, M., Li, Z., Liu, F., Sousa, A.M.M., Nakagawa, N., Li, M., Dell'Anno, M.T., Gulden, F.O., Pochareddy, S., Tebbenkamp, A.T.N., et al. (2016). Zika virus disrupts phospho-TBK1 localization and mitosis in human neuroepithelial stem cells and radial glia. *Cell Rep.* 16, 2576–2592.
- Pellegrini, E., Desfosses, A., Wallmann, A., Schulze, W.M., Rehbein, K., Mas, P., Signor, L., Gaudon, S., Zenkeviciute, G., Hons, M., et al. (2018). RIP2 filament formation is required for NOD2 dependent NF-kappaB signalling. *Nat. Commun.* 9, 4043.
- Pillai, S., Nguyen, J., Johnson, J., Haura, E., Coppola, D., and Chellappan, S. (2015). Tank binding kinase 1 is a centrosome-associated kinase necessary for microtubule dynamics and mitosis. *Nat. Commun.* 6, 10072.
- Pilli, M., Arko-Mensah, J., Ponpuak, M., Roberts, E., Master, S., Mandell, M.A., Dupont, N., Ornatowski, W., Jiang, S., Bradfute, S.B., et al. (2012). TBK-1 promotes autophagy-mediated antimicrobial defense by controlling autophagosome maturation. *Immunity* 37, 223–234.
- Pottier, C., Bieniek, K.F., Finch, N., van de Vorst, M., Baker, M., Perkersen, R., Brown, P., Ravenscroft, T., van, B.M., Nicholson, A.M., et al. (2015). Whole-genome sequencing reveals important role for TBK1 and OPTN mutations in frontotemporal lobar degeneration without motor neuron disease. *Acta Neuropathol.* 130, 77–92.
- Pourcelot, M., Zemirli, N., Silva Da, C.L., Loyant, R., Garcin, D., Vitour, D., Munitic, I., Vazquez, A., and Arnould, D. (2016). The Golgi apparatus acts as a platform for TBK1 activation after viral RNA sensing. *BMC Biol.* 14, 69.
- Rai, A.K., Chen, J.X., Selbach, M., and Pelkmans, L. (2018). Kinase-controlled phase transition of membraneless organelles in mitosis. *Nature* 559, 211–216.
- Ramaswami, M., Taylor, J.P., and Parker, R. (2013). Altered ribostasis: RNA-protein granules in degenerative disorders. *Cell* 154, 727–736.
- Reineke, L.C., and Lloyd, R.E. (2013). Diversion of stress granules and P-bodies during viral infection. *Virology* 436, 255–267.
- Rizzolo, K., Huen, J., Kumar, A., Phanse, S., Vlasblom, J., Kakiyama, Y., Zeineddine, H.A., Minic, Z., Snider, J., Wang, W., et al. (2017). Features of the chaperone cellular network revealed through systematic interaction mapping. *Cell Rep.* 20, 2735–2748.
- Ro, S.H., Jung, C.H., Hahn, W.S., Xu, X., Kim, Y.M., Yun, Y.S., Park, J.M., Kim, K.H., Seo, M., Ha, T.Y., et al. (2013). Distinct functions of Ulk1 and Ulk2 in the regulation of lipid metabolism in adipocytes. *Autophagy* 9, 2103–2114.
- Roe, S.M., Prodromou, C., O'Brien, R., Ladbury, J.E., Piper, P.W., and Pearl, L.H. (1999). Structural basis for inhibition of the Hsp90 molecular chaperone by the antitumor antibiotics radicicol and geldanamycin. *J. Med. Chem.* 42, 260–266.
- Ryzhakov, G., and Randow, F. (2007). SINTBAD, a novel component of innate antiviral immunity, shares a TBK1-binding domain with NAP1 and TANK. *EMBO J.* 26, 3180–3190.
- Saito, M., Hess, D., Eglinger, J., Fritsch, A.W., Kreysing, M., Weinert, B.T., Choudhary, C., and Matthias, P. (2019). Acetylation of intrinsically disordered regions regulates phase separation. *Nat. Chem. Biol.* 15, 51–61.
- Saitoh, T., Fujita, N., Hayashi, T., Takahara, K., Satoh, T., Lee, H., Matsunaga, K., Kageyama, S., Omori, H., Noda, T., et al. (2009). Atg9a controls dsDNA-driven dynamic translocation of STING and the innate immune response. *Proc. Natl. Acad. Sci. U S A* 106, 20842–20846.
- Saunders, T.E., Pan, K.Z., Angel, A., Guan, Y., Shah, J.V., Howard, M., and Chang, F. (2012). Noise reduction in the intracellular pom1p gradient by a dynamic clustering mechanism. *Dev. Cell* 22, 558–572.
- Schmitz, M.L., Kracht, M., and Saul, V.V. (2014). The intricate interplay between RNA viruses and NF-kappaB. *Biochim. Biophys. Acta* 1843, 2754–2764.
- Seo, M., Lee, S.O., Kim, J.H., Hong, Y., Kim, S., Kim, Y., Min, D.H., Kong, Y.Y., Shin, J., and Ahn, K. (2016). MAP4-regulated dynein-dependent trafficking of BTN3A1 controls the TBK1-IRF3 signaling axis. *Proc. Natl. Acad. Sci. U S A* 113, 14390–14395.
- Sharma, S., tenOever, B.R., Grandvaux, N., Zhou, G.P., Lin, R., and Hiscott, J. (2003). Triggering the interferon antiviral response through an IKK-related pathway. *Science* 300, 1148–1151.
- Shi, C.S., and Kehrl, J.H. (2010). TRAF6 and A20 regulate lysine 63-linked ubiquitination of Beclin-1 to control TLR4-induced autophagy. *Sci. Signal.* 3, ra42.
- Taylor, J.P., Brown, R.H., Jr., and Cleveland, D.W. (2016). Decoding ALS: from genes to mechanism. *Nature* 539, 197–206.
- Thurston, T.L., Ryzhakov, G., Bloor, S., von, M.N., and Randow, F. (2009). The TBK1 adaptor and autophagy receptor NDP52 restricts the proliferation of ubiquitin-coated bacteria. *Nat. Immunol.* 10, 1215–1221.
- Uversky, V.N. (2017). Intrinsically disordered proteins in overcrowded milieu: membrane-less organelles, phase separation, and intrinsic disorder. *Curr. Opin. Struct. Biol.* 44, 18–30.
- Uversky, V.N., and Dunker, A.K. (2010). Understanding protein non-folding. *Biochim. Biophys. Acta* 1804, 1231–1264.
- Vajjhala, P.R., Ve, T., Bentham, A., Stacey, K.J., and Kobe, B. (2017). The molecular mechanisms of signaling by cooperative assembly formation in innate immunity pathways. *Mol. Immunol.* 86, 23–37.
- Wheeler, R.J., and Hyman, A.A. (2018). Controlling compartmentalization by non-membrane-bound organelles. *Philos. Trans. R. Soc. Lond. B Biol. Sci.* 373, pii: 20170193.
- Wild, P., Farhan, H., McEwan, D.G., Wagner, S., Rogov, V.V., Brady, N.R., Richter, B., Korac, J., Waidmann, O., Choudhary, C., et al. (2011). Phosphorylation of the autophagy receptor optineurin restricts Salmonella growth. *Science* 333, 228–233.
- Wippich, F., Bodenmiller, B., Trajkovska, M.G., Wanka, S., Aebersold, R., and Pelkmans, L. (2013). Dual specificity kinase DYRK3 couples stress granule condensation/dissolution to mTORC1 signaling. *Cell* 152, 791–805.
- Woodruff, J.B., Ferreira, G.B., Widlund, P.O., Mahamid, J., Honigsmann, A., and Hyman, A.A. (2017). The centrosome is a selective condensate that nucleates microtubules by concentrating tubulin. *Cell* 169, 1066–1077.
- Xu, D., Jin, T., Zhu, H., Chen, H., Ofengeim, D., Zou, C., Mifflin, L., Pan, L., Amin, P., Li, W., et al. (2018). TBK1 suppresses RIPK1-driven apoptosis and inflammation during development and in aging. *Cell* 174, 1477–1491.
- Yang, K., Shi, H., Qi, R., Sun, S., Tang, Y., Zhang, B., and Wang, C. (2006). Hsp90 regulates activation of interferon regulatory factor 3 and TBK-1 stabilization in Sendai virus-infected cells. *Mol. Biol. Cell* 17, 1461–1471.
- Zhao, P., Wong, K.I., Sun, X., Reilly, S.M., Uhm, M., Liao, Z., Skorobogatko, Y., and Saltiel, A.R. (2018). TBK1 at the crossroads of inflammation and energy homeostasis in adipose tissue. *Cell* 172, 731–743.
- Zhu, L., Xie, X., Zhang, L., Wang, H., Jie, Z., Zhou, X., Shi, J., Zhao, S., Zhang, B., Cheng, X., and Sun, S.C. (2018). TBK-binding protein 1 regulates IL-15-induced autophagy and NKT cell survival. *Nat. Commun.* 9, 2812.

ISCI, Volume 19

Supplemental Information

**ULK1/2 Restricts the Formation of Inducible
SINT-Speckles, Membraneless Organelles
Controlling the Threshold of TBK1 Activation**

Vera Vivian Saul, Markus Seibert, Marcus Krüger, Sylvia Jeratsch, Michael Kracht, and Michael Lienhard Schmitz

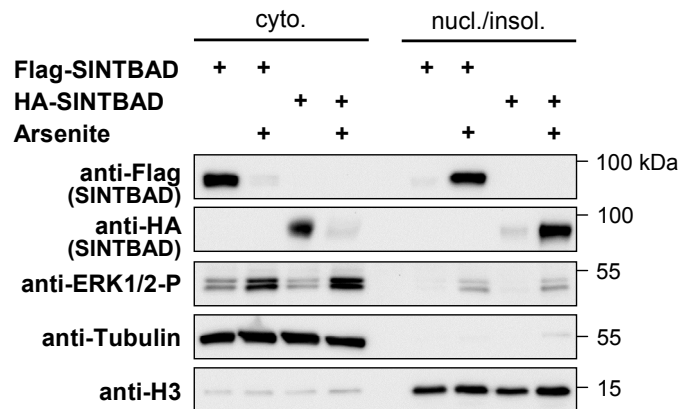
Supplemental information

ULK1/2 restrict the formation of inducible SINT-speckles, membrane-less organelles controlling the threshold of TBK1 activation

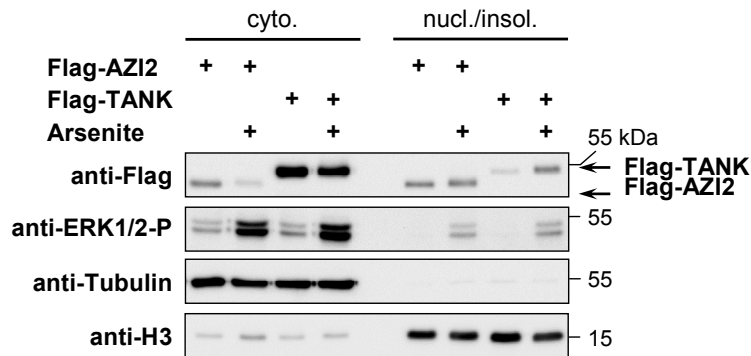
Vera V. Saul, Markus Seibert, Marcus Krüger, Sylvia Jeratsch, Michael Kracht and M. Lienhard SCHMITZ

Supplementary figures

S1 A



B



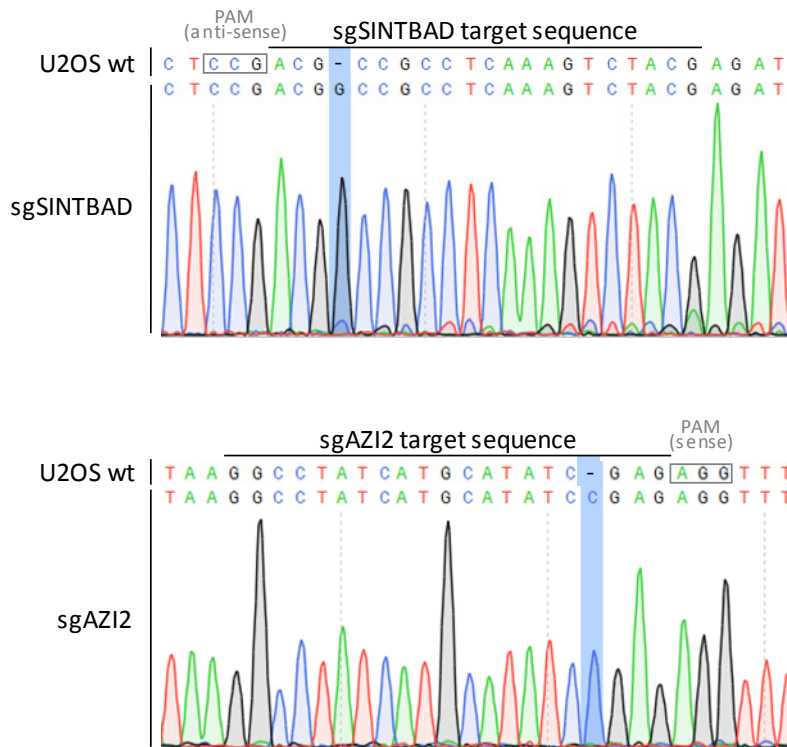
Suppl. Fig. S1. Relocalization of adapter proteins in response to cell stress, Related to Figure 1. 293T cells were transfected to express Flag- or HA-tagged SINTBAD (**A**) or AZI2 and TANK (**B**) as shown. Cells were stimulated with 0.5 mM arsenite for 1 h, harvested and fractionated into cytosolic (cyto.) and nuclear/insoluble (nucl./insol.) extracts. Western blotting was performed to detect the adapter proteins, controls for successful cell fractionation (histone H3 and Tubulin) and cell stimulation (ERK1/2-P). The positions of molecular weight markers are indicated.

Supplementary figures

S2 A



B

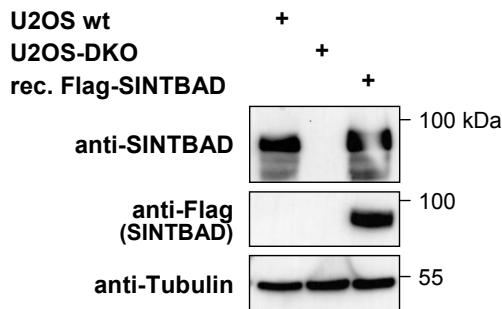


Suppl. Fig. S2. Generation of SINTBAD- and/or AZI2-deficient U2OS cells, Related to Figure 1. (A) U2OS cells were transfected with a px459 plasmid encoding a sgRNA targeting the second exon of the AZI2 gene or the first exon of SINTBAD. After selection of non-transfected cells with Puromycin, individual cell clones were grown and analyzed by Western blotting using AZI2- and SINTBAD-specific antibodies. The AZI2 antibody also detects a non-specific band which is indicated by an asterisk. Double-deficient U2OS cells were generated by transfecting the sgRNA against AZI2 into SINTBAD knockout cells. **(B)** Genomic DNA was isolated from SINTBAD-deficient cell clones and double-knockout cells. The respective genomic region encompassing the Cas9 cleavage site was amplified by PCR and sequenced as shown. The position of homozygous insertion of a nucleotide base in comparison to the wt sequence is highlighted in blue.

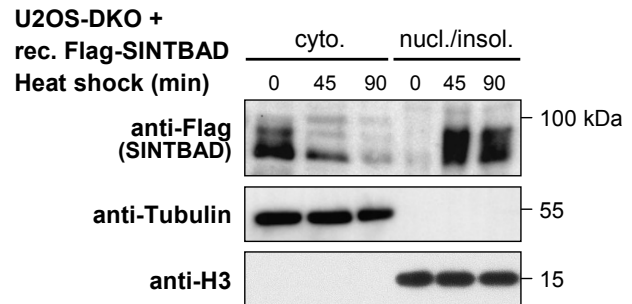
Supplementary figures

S3

A

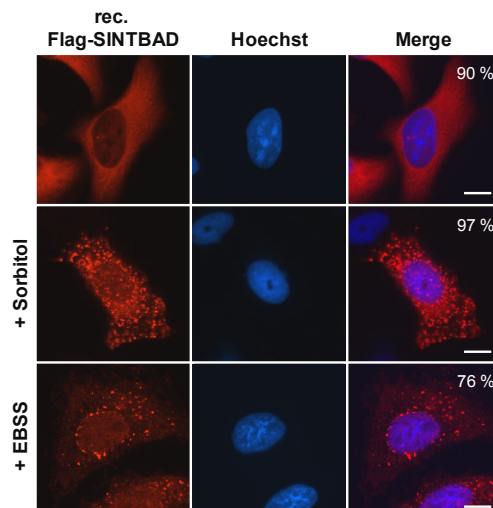


B



Suppl. Fig. S3. Characterization of U2OS-sgAZI2/sgSINTBAD (U2OS-DKO) cells reconstituted to stably express Flag-SINTBAD, Related to Figure 1. (A) U2OS wt cells, U2OS-sgAZI2/sgSINTBAD double knock-out (DKO) cells and their derivative cell clone reconstituted to stably express Flag-SINTBAD were lysed and tested by Western blot analysis for expression of Flag-tagged SINTBAD as shown. (B) U2OS-sgAZI2/sgSINTBAD cells reconstituted to stably express Flag-SINTBAD were exposed to heat shock for the indicated periods. Cells were harvested and fractionated into cytosolic (cyto.) and nuclear/insoluble (nucl./insol.) extracts. Western blotting was performed to detect the dynamic relocalization of Flag-SINTBAD, the detection of histone H3 and Tubulin show the purity of cell fractions.

S4

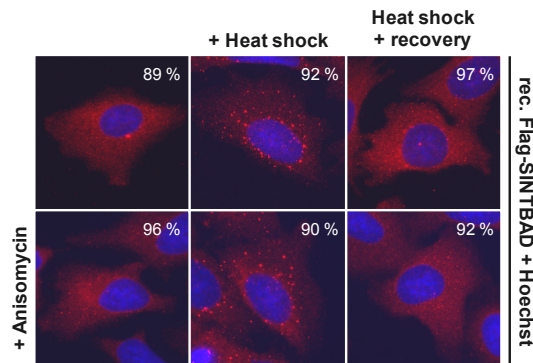


Suppl. Fig. S4. Analysis of stress-induced SINTBAD relocalization, Related to Figure 1. U2OS-sgAZI2/sgSINTBAD cells reconstituted to stably express Flag-SINTBAD were treated with 0.5 M sorbitol for 1 h or the starvation medium EBSS (Axe et al., 2008) for 4 h and analyzed by indirect immunofluorescence for the intracellular distribution of SINTBAD. Scale bar = 10 μ m, the percentage of cells showing the displayed phenotype is indicated.

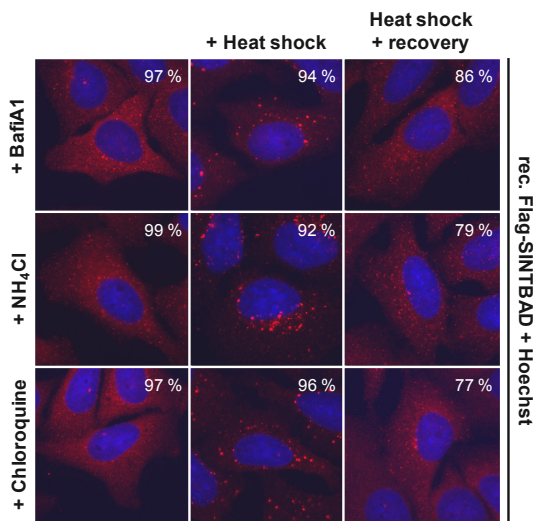
Supplementary figures

S5

A



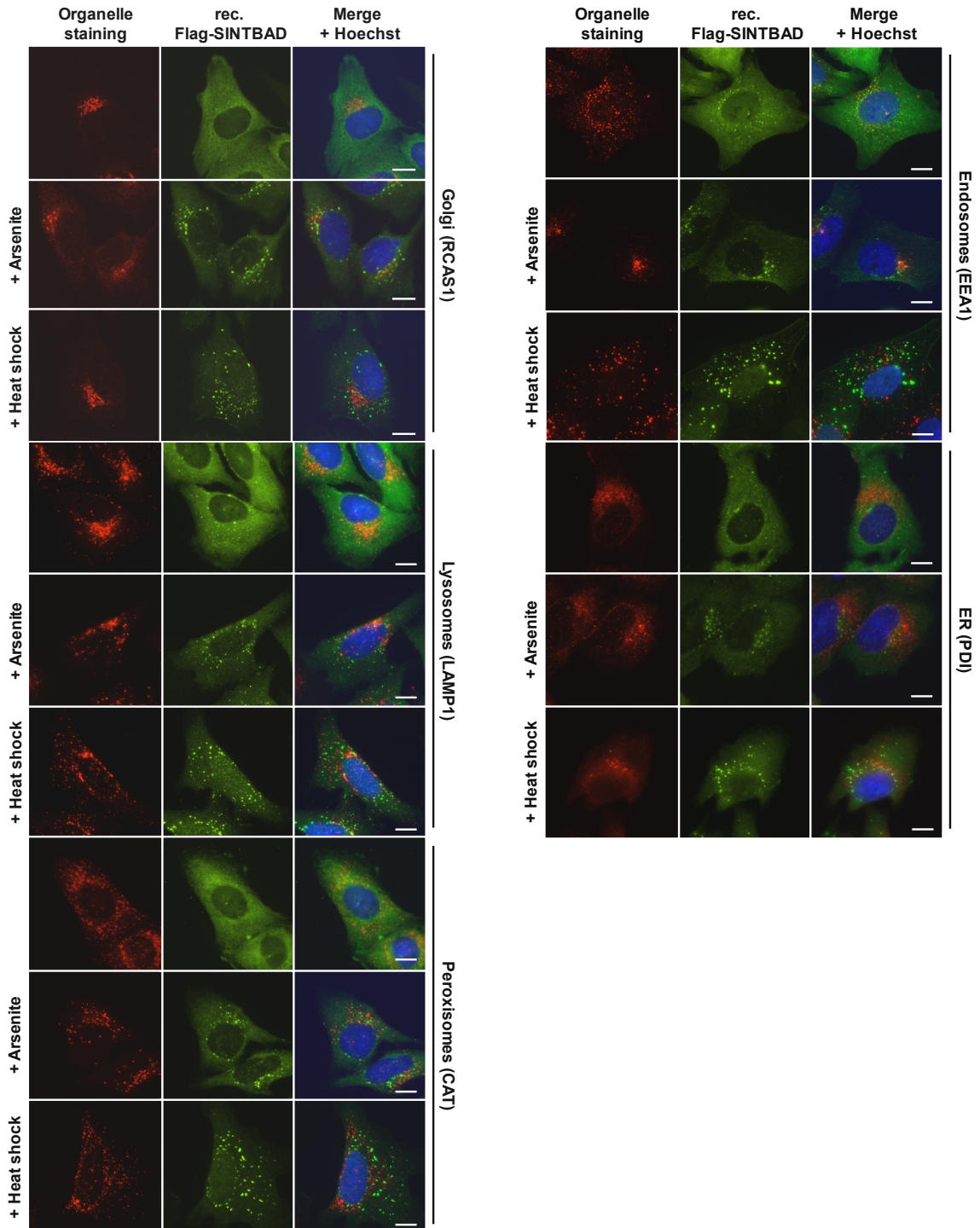
B



Suppl. Fig. S5. Disaggregation of heat shock-induced SINT-speckles is independent of de novo protein expression and autophagy, Related to Figure 3. (A) SINTBAD-deficient U2OS cells reconstituted with Flag-SINTBAD were left untreated or exposed to heat shock. Indicated cells were allowed to recover from heat shock at 37 °C for 3 h in the absence or presence of the translation inhibitor anisomycin (5 µg/ml). (B) SINTBAD-deficient U2OS cells stably expressing Flag-SINTBAD were left untreated or exposed to heat shock, followed by a 3 h long recovery period at 37 °C. Treatments and recovery were performed in the presence of the indicated autophagy inhibitors (0.5 µM Bafilomycin A, 20 mM NH₄Cl, 20 µM Chloroquine). The percentage of cells showing the displayed phenotype is indicated.

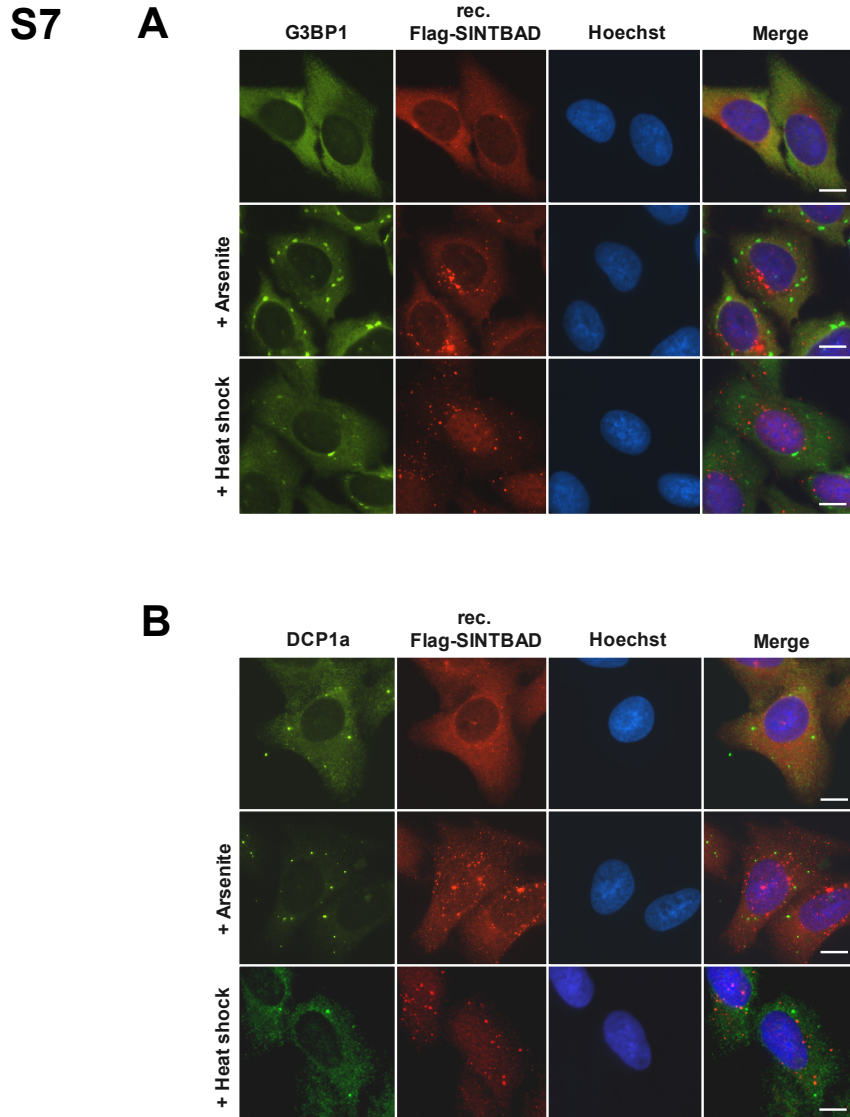
Supplementary figures

S6



Suppl. Fig. S6. SINTBAD does not colocalize with membrane-surrounded organelles, Related to Figure 4. U2OS cells stably expressing Flag-SINTBAD were treated with arsenite, exposed to heat shock or left untreated as shown. Immunofluorescence studies were performed by costaining Flag-SINTBAD together and the indicated marker proteins for Golgi (RCAS1), lysosomes (LAMP1), peroxisomes (CAT), endosomes (EEA1) and endoplasmic reticulum (PDI). Representative pictures are shown. Scale bars = 10 μm.

Supplementary figures



Suppl. Fig. S7. SINTBAD does not colocalize with or influence the formation of other MLOs, Related to Figure 4. Reconstituted U2OS cells were left untreated or exposed to arsenite or heat shock. Costaining of Flag-SINTBAD with G3BP1 (**A**) or DCP1a (**B**) allowed the analysis of the occurrence of stress granules and P bodies, respectively. Scale bars = 10 μ m.

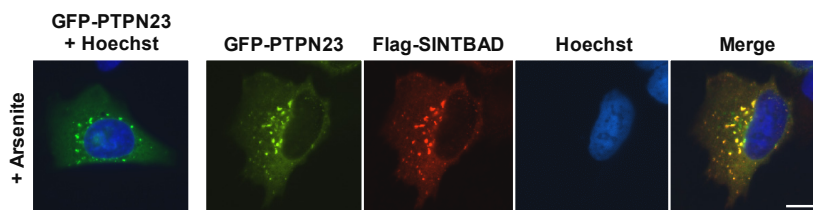
Supplementary figures

S8

A

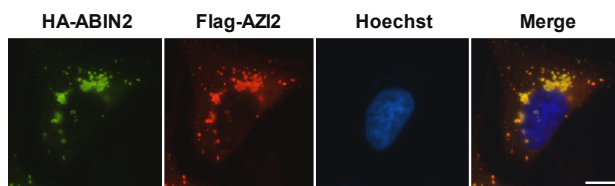
IP	Group 1	Group 2a	Group 2b
control IgG	no detection in both experiments	detected in both experiments	detected in one experiment
anti-Flag Ab	detected in both experiments		
Threshold for SINTBAD interactome (+ min. 1 unique peptide in both experiments)	interactors defined by $>25.5 \log_2$ intensity	interactors defined by $>2 \log_2$ fold-change & $>1,3 -\log_{10}$ p-value	interactors defined by $>4 \log_2$ fold-change enrichment in comparison to median of control IgG

B



Suppl. Fig. S8. Characterization of SINTBAD interactors, Related to Figure 5. (A) 293T cells were transfected to express Flag-SINTBAD and co-immunoprecipitation experiments were performed. After identification of co-immunoprecipitating proteins by mass spectrometry, the specifically interacting proteins were defined according to the criteria indicated above. (B) U2OS cells were transfected to express the SINTBAD interactor PTPN23 either alone or together with Flag-tagged SINTBAD, followed by treatment with arsenite as shown. Immunofluorescence was used to reveal the intracellular localization of the proteins. Scale bar = 10 μ m.

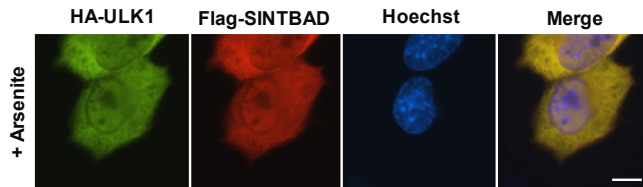
S9



Suppl. Fig. S9. Analysis of ABIN2/AZI2 interaction, Related to Figure 6. U2OS cells were transfected to express HA-ABIN and Flag-AZI2 and analyzed by immunofluorescence. Scale bar = 10 μ m.

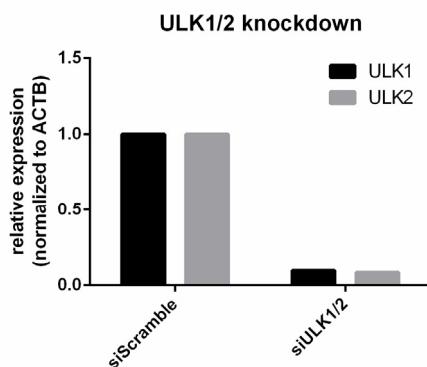
Supplementary figures

S10



Suppl. Fig. S10. ULK1 restricts SINT-speckle formation, Related to Figure 6. U2OS cells were transfected to express HA-ULK1 together with Flag-SINTBAD. Cells were treated with arsenite and analyzed by indirect immunofluorescence. A representative experiment is shown, nuclear DNA was stained with Hoechst. Scale bar = 10 μ m.

S11

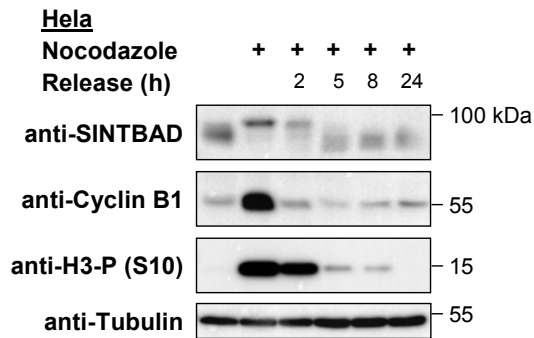


Suppl. Fig. S11. Characterization of ULK1/2 knockdown, Related to Figure 7. Reconstituted U2OS cells stably expressing Flag-SINTBAD were treated with ULK1- and ULK2-specific Accell siRNAs. Three days after siRNA transfection, one aliquot of the cells was analyzed for efficient mRNA knockdown by qPCR using primers specific for ULK1 and ULK2, respectively. Gene expression values were normalized to transcription of the β -Actin encoding gene (ACTB), ULK1/2 expression in the control cells transfected with scrambled siRNAs was set as 1.

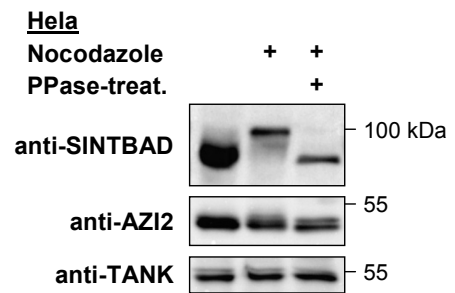
Supplementary figures

S12

A



B

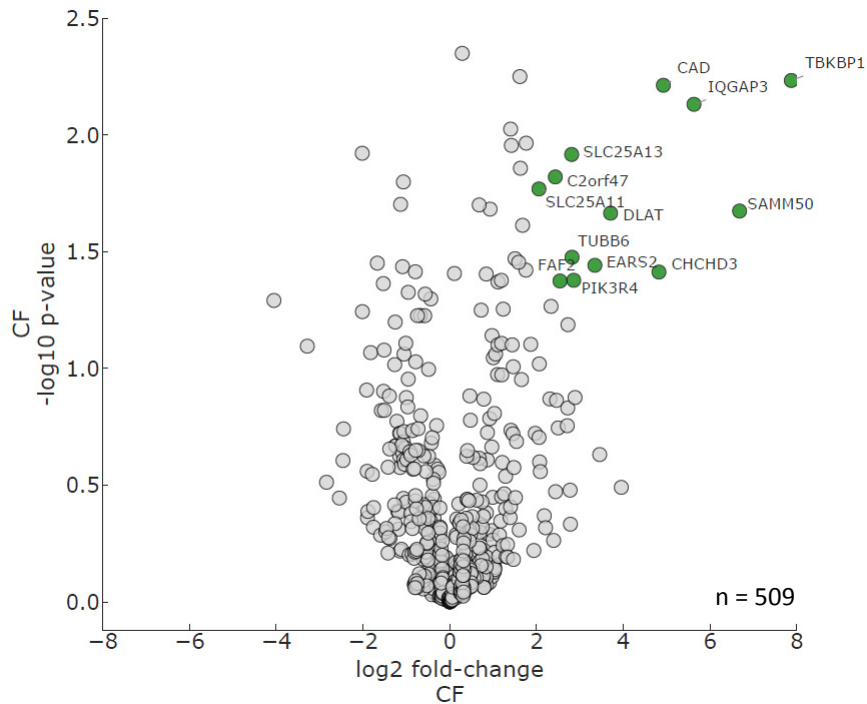


Suppl. Fig. S12. Characterization of mitotic SINTBAD phosphorylation, Related to Figure 7. (A) HeLa cells were arrested in prometaphase by adding 100 ng/ml nocodazole for 15 h. Cells were washed with PBS and further grown in DMEM for the indicated time periods. Cell extracts were tested for the electrophoretic behavior of the indicated proteins, the retarded migration of the phosphorylated SINTBAD protein (SINTBAD-P) is shown. Cyclin B1 and phosphorylated histone H3 (Ser10) were detected to ensure successful mitotic synchronization and release of cells. **(B)** To prove that the upshift of the SINTBAD band is caused by phosphorylation, SINTBAD extracted from nocodazole-arrested HeLa cells was incubated with λ phosphatase (PPase, 400 U, 30 min at 30 °C) as indicated and proteins were analyzed for their electrophoretic behavior by Western blotting as shown.

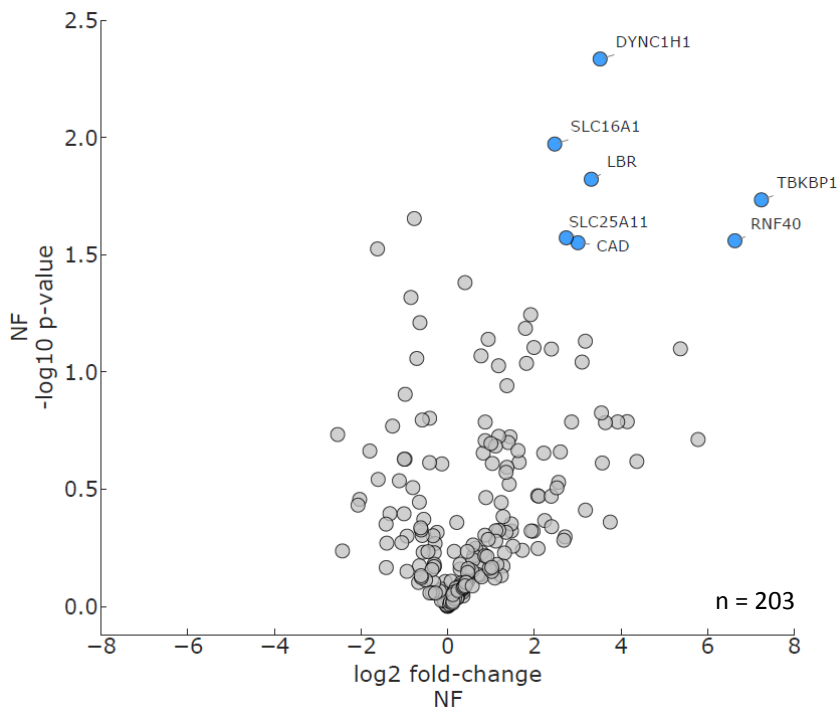
Supplementary figures

S13

A



B



Suppl. Fig. S13. Analysis of the SINTBAD interactome, Related to transparent methods. Volcano plot analysis of the Group 2a interactors according to the definitions given in table 1. Interactors of the cytosolic fraction (CF) (A) or the nuclear/insoluble fraction (NF) (B) were plotted according to their log₂ fold-enrichment and -log₁₀ p-values as shown. The selected proteins considered as SINTBAD interactors are named and indicated by colors.

TRANSPARENT METHODS

Reagents and primary antibodies

The following reagents were purchased from the indicated companies: Anisomycin (A9789, Sigma-Aldrich), Bafilomycin A (tlrl-baf1, Invivogen), Chloroquine (C6628, Sigma-Aldrich), Geldanamycin (HN71, Carl Roth), IL-1 β (gift from M. Kracht), LPS (L4130, Sigma-Aldrich), Nocodazole (M1404, Sigma-Aldrich), Pifithrin- μ (BML-AP503, Enzo Life Sciences), Radicicol (BN0437, Biotrend), Sodium (meta)arsenite (71287, Sigma-Aldrich), Sorbitol (S1876, Sigma-Aldrich), TNF α (11343015, ImmunoTools) Ver155008 (SML0271, Sigma-Aldrich). The following antibodies were used in this study: anti-AZI2 (WB: 1:1000, ab192253, Abcam), anti-CAT (IF: 1:400, #12980, Cell Signaling), anti-c-Myc (IF: 1:1000, WB: 1:2000, sc-40, Santa Cruz Biotechnology), anti-Cyclin B1 (WB: 1:500, GSN11, Thermo Fisher Scientific), anti-DCP1a (IF: 1:200, sc-100706, Santa Cruz Biotechnology), anti-eIF4G (IF: 1:200, sc-133155, Santa Cruz Biotechnology), anti-ERK1/2-P (T202/Y204-P; WB: 1:1000, #9101, Cell Signaling), anti-Flag M2 (IF: 1:2000, WB: 1:5000, F3165, Sigma-Aldrich), anti-G3BP1 (IF: 1:400, sc-81940, Santa Cruz Biotechnology), anti-HA (IF: 1:500, WB: 1:1000, 11867423001, Roche), anti-Histone H3 (WB: 1:5000, ab1791, Abcam), anti-Histone H3-P (S10-P; WB: 1:1000, #9706, Cell Signaling), anti-p38-P (T180/Y182-P; WB: 1:1000, #9211, Cell Signaling), anti-SINTBAD (WB: 1:1000, #8615, Cell Signaling), anti-TBK1 (IF: 1:200, WB: 1:5000, ab40676, Abcam), anti-TBK1-P (S172-P; IF: 1:150, WB: 1:1000, #5483, Cell Signaling), anti-TANK (WB: 1:400, sc-166643, Santa Cruz Biotechnology), anti-Tubulin (WB: 1:1000, E7, DSHB), Organelle Localization IF Antibody Sampler Kit including antibodies detecting AIFM1, EEA1, LAMP1, PDI and RCAS1 (#8653, Cell Signaling).

Plasmids

SINTBAD was cloned by PCR from a human sequence-verified cDNA clone pBSII-SK(+)-TBKBP1 (BC167150, Biocat) along with an N-terminal epitope tag into the pcDNA3.1 vector (Invitrogen). Flag-SINTBAD truncation mutants were generated by cloning a PCR-amplified fragment into pcDNA3.1 (Δ N1: 106-615 aa, Δ N2: 165-615 aa, Δ C: 1-520 aa). Expression plasmids for Flag-TANK, Flag-AZI2 and Myc-TBK1 were kindly provided by Dr. A. Chariot (University of Liège, Belgium, (Chariot et al., 2002)); plasmids expressing HA-HSP70 and Flag-HSP90 were from Dr. B. Song (Emory University School of Medicine, Atlanta, USA, (Hwang et al., 2010)); pEGFP-C2-PTPN23 was obtained from Dr. C. A. Tanase (University of Bucharest, Romania, (Tanase, 2010)); pEGFP-AMBRA1 was generated by subcloning the

coding sequence of pLPCX-Ambra1-Flag (Dr. F. Cecconi, University of Rome, Italy, (Nazio et al., 2013)) into the pEGFP-C2 vector (Clontech); PCR-amplified ABIN2 from pCAGGS-E-hABIN2, that was kindly provided by Dr. R. Beyaert (VIB-Ghent University, Belgium, (Van et al., 2001)) was subcloned with a N terminal HA-tag into pcDNA6 (Invitrogen); pcDNA3.1-HA-ULK1 was obtained from Dr. S. H. Tooze (The Francis Crick Institute, London, UK, (Joachim et al., 2015)) and its kinase-inactive K46I mutant was generated by site-directed mutagenesis (QuikChange II XL, Agilent, (Chan et al., 2009)). Flag-KAT2A was from Dr. Ezra Burstein (UT Southwestern, Dallas, USA, (Mao et al., 2009)) and pIRES-3x-Flag-NSs (SFTSV) from Dr. J. U. Jung (University of Southern California, Los Angeles, USA, (Choi et al., 2019)).

Cell culture, transfections and treatments

293T, HEK-TLR4, HeLa and U2OS cells were cultured in DMEM (Gibco) containing high glucose (4.5 g/l), L-alanyl-glutamine (4 mM) and sodium pyruvate (110 mg/l) supplemented with 10 % fetal bovine serum (FBS), 100 U/ml penicillin and 100 µg/ml streptomycin. Cells were grown in a humidified incubator at 37 °C under 5 % CO₂. Transient transfections of plasmids were performed using linear polyethylenimine (PEI, Polyscience Inc.) as described previously (Saul et al., 2015). Unless indicated otherwise, cells were treated with 0.5 mM arsenite for 1 h or were exposed to heat shock at 43 °C in a humidified cell culture incubator with a 5 % CO₂ atmosphere for 1 h. Inhibitors were incubated 1 h prior cell stimulation. Cell stimulations for the experiments displayed in Fig. 1C were done as follows: HeLa cells were treated with 0.5 M sorbitol (30, 60, 90 min), 0.5 mM arsenite (20, 40, 60 min) or 4 % (v/v) ethanol (15, 30 and 60 min). In addition, HEK-TLR4 cells were treated with 1 µg/ml LPS (1, 2, 4 h), U2OS cells with 10 ng/ml IL-1β (0.5, 1.5, 5 h) and HEK293 cells with 20 ng/ml TNFα (30, 60, 90 min).

Generation of CRISPR/Cas9-mediated knockout cells and reconstitution of them

In order to generate SINTBAD- and/or AZI2-deficient U2OS cells, CRISPR/Cas9-mediated genome editing technology was performed as described (Ran et al., 2013). The target site for human SINTBAD was designed as an anti-sense sgRNA (5'-CGTAGACTTTGAGGCGGCGT-3') within the first exon of the SINTBAD gene. The target site for sgAZI2 was designed within the second exon as 5'-GGCCTATCATGCATATCGAG-3'. Oligos were ligated into px459 V2.0 vector (Addgene plasmid #62988) using standard protocols and verified by sequencing. U2OS cells, seeded in a 6 cm dish, were transfected

with 1 µg of empty px459 or px459-sgRNA vector. One day after transfection, cells were selected for 30 h using 1 µg/ml Puromycin (Invivogen), diluted and further grown to allow the formation of single-cell clones. These clones were picked and analyzed for SINTBAD, AZI2 and Cas9 expression and verified by sequencing of the genomic DNA at the appropriate locus. To obtain SINTBAD/AZI2 double-deficient cells, a SINTBAD-deficient cell clone was transfected with px459-sgAZI2 and selected as described above. To reconstitute SINTBAD-deficient U2OS cells, cells were transfected with an pcDNA3.1/zeo-Flag-SINTBAD expression construct and continuously selected using 400 µg/ml Zeocin (Invivogen). Single-cell clones were picked and analyzed by Western blotting.

Knockdown of ULK1 and ULK2

Reconstituted U2OS cells stably expressing Flag-SINTBAD were treated with 1 µM ULK1 and ULK2-specific Accell siRNAs (Dharmacon #A-005049-13-0005 and #A-005396-14-0005) or with a scrambled control RNA (Seibert et al., 2019) according to the protocol using Accell siRNA Delivery Media (Dharmacon #B-005000-500). Three days after siRNA transfection, half of the cells were seeded on coverslips and used for immunofluorescence staining and the remaining cells were analyzed for efficient knockdown by real time qPCR, using the following primers specific for ACTB (5'-CATGTACGTTGCTATCCAGGC-3', 5'-CTCCTTAATGTACGCACGAT-3'), ULK1 (5'-ACCCATTACTGCGAACCTGGA-3', 5'-GCACGAACAGCAGCGTGAAGC-3') and ULK2 (5'-TCTGCATCACCATGTGCAAGAA-3', 5'-AACATCTCATCCAGGGCT-3').

Cell lysis protocols and subcellular fractionation

To prepare cell lysates under native conditions, cells were lysed on ice for 20 min in IGEPAL buffer (20 M Tris/HCl pH 7.5, 150 mM NaCl, 1 % IGEPAL CA-630 (Sigma-Aldrich), 5 % glycerol and freshly added 10 mM NaF, 0.5 mM Na₃VO₄, 1 mM PMSF, 5 µg/ml leupeptin and 5 µg/ml aprotinin). The lysates were cleared by centrifugation and the supernatants were transferred into a fresh tube and either used for coimmunoprecipitation studies or mixed with sample buffer for Western blot analysis. To lyse cells under denaturing conditions, the washed cell pellets were resuspended in 1 × SDS sample buffer and sonicated two times for 20 sec with a Branson sonifier to shear the genomic DNA. After boiling the samples for 5 min, the lysates were analyzed by Western blotting. For subcellular fractionation experiments, cells, grown and treated in a 6 cm dish, were lysed in 160 µl low-salt buffer (10 mM Hepes, pH 7.9, 10 mM KCl, 0.1 mM EDTA, 0.1 mM EGTA, 1 mM β-mercaptoethanol and 0.5 mM freshly

added PMSF) on ice for 10 min. NP-40 (Roche) was added to a final concentration of 0.25 %, samples were briefly vortexed and centrifuged for 10 sec at $16\,000 \times g$. The supernatants representing the cytoplasmic fractions were collected in fresh tubes and mixed with $5 \times$ SDS sample buffer. The remaining pellets representing the nuclear/insoluble fractions were washed twice in low-salt buffer and then resuspended in $180 \mu\text{l}$ $1 \times$ SDS sample buffer, boiled and sheared two times for 20 sec with a sonifier. The purity of the cellular fractions was confirmed by Western blotting, detecting Tubulin and histone H3 as markers for the cytosolic or nuclear/insoluble fraction, respectively.

Coimmunoprecipitation experiments and Western blotting

For coimmunoprecipitation, cleared cell extracts lysed in IGEPAL lysis buffer were filled up to a volume of $600 \mu\text{l}$ with lysis buffer and supplemented with $1 \mu\text{g}$ precipitating antibody or control IgG. After adding $20 \mu\text{l}$ protein A/G agarose (Millipore), the samples were incubated for 4 h at 4°C on a rotating wheel. Alternatively, covalently antibody-coupled affinity gels were used for coimmunoprecipitation (anti-Flag M2 affinity gel, A2220, Sigma-Aldrich; GFP-Trap_A, Chromotek). Agarose beads were then washed four times with 1 ml cold IGEPAL buffer. Precipitated proteins were eluted by adding $1.5 \times$ SDS sample buffer. Equal amounts of protein were separated by SDS-PAGE, followed by semidry blotting to a PVDF membrane (IPVH00010, Millipore). Further analysis was performed using standard methods. After blocking the membrane, primary antibodies, diluted in 2 % nonfat dry milk or 5 % BSA (Sigma-Aldrich) in TBST, were incubated overnight at 4°C . Peroxidase-coupled antibodies (Jackson ImmunoResearch) were diluted 1:5000 in 2 % dry milk in TBST and incubated 2 h at room temperature. Immunoreactive bands were detected using the Western Lightning Plus-ECL reagent (Perkin Elmer) and visualized on a ChemiDoc Imaging System (Bio-Rad).

Immunofluorescence staining

U2OS cells or their derivatives were grown on coverslips in 12- or 24-well plates. Cells were transfected and/or treated as indicated and described in the figure legend. After washing the cells with PBS, cells were fixed for 1 min with ice-cold methanol/acetone (1:1). After rehydration, the cells were blocked with 5 % BSA in PBS for 1 h at room temperature. Coverslips were subsequently incubated with the indicated primary antibodies, diluted in PBS containing 1 % BSA and 0.1 % Triton X-100, for 90 min at room temperature or at 4°C overnight. After washing three times with PBS cells were incubated with the appropriate secondary Alexa488- or Cy3-conjugated antibodies (Jackson ImmunoResearch) diluted

1:3000 in 1 % BSA in PBS for 90 min in the dark. After incubation, cells were washed three times in PBS and the nuclear DNA was stained with Hoechst 33324 (Invitrogen). The samples were mounted with Mowiol mounting medium and stored at 4 °C. Analysis of the stained cells was done using an Eclipse TE2000-E microscope (Nikon) and a 63 × oil-immersion lens. For each condition >30 healthy individual cells were analyzed and pictures of one representative cell were taken with an OCRA-spark digital CMOS camera (C11440-36U, Hamamatsu). For the quantification of protein localizations and cellular phenotypes, at least 100 cells for each condition were analyzed.

Mass spectrometry

To identify SINTBAD interactors by mass spectrometry, 293T cells were either transfected with the pcDNA3.1-Flag-SINTBAD expression construct or the empty vector. Four 10 cm dishes for each condition were taken for large-scale immunoprecipitation. Washed cells were harvested and lysed in 1 ml low-salt buffer as described above. The received cytosolic fraction was mixed with 1 ml IGEPAL lysis buffer, containing Complete Protease Inhibitor Cocktail and PhosSTOP (Roche). The remaining cell pellet was washed two times in low-salt buffer and then resuspended in 2 ml IGEPAL lysis buffer and sonified two times for 20 sec. The two fractions were precleared by incubating them 1 h with 3 µg control mouse IgG (Santa Cruz Biotechnology) and 40 µl Protein A/G Agarose. Afterwards, immunoprecipitation was performed by incubating the lysates with 6 µg anti-Flag M2 antibodies together with 80 µl Agarose beads for 4 h at 4 °C on a rotating wheel. Beads were washed five times with 2 ml IGEPAL lysis buffer, transferred to a fresh tube and proteins were eluted at 70 °C for 10 min in LDS sample buffer (Invitrogen). Samples were separated on a 4-12 % Bis-Tris gradient-gel (NuPAGE, Invitrogen), stained with colloidal Coomassie (Invitrogen) and cut into small pieces (7 slides each lane). In-gel digestion of the proteins with trypsin and purification of the peptides was performed as described (Seibert et al., 2019). Peptide solutions were desalted by stop and go extraction (STAGE) tips (Rappsilber et al., 2003). The purification and mass spectrometry of two individual experiments was performed with a time lag and therefore analyzed with different instrumental settings. Dissenting setting parameters of analysis 1 and 2 are indicated by a slash. Samples were eluted from STAGE tips with acetonitrile and applied to the UHPLC system (EASY-nLC 1000, Thermo Fisher Scientific) in 0.1 % formic acid. Separation of peptides by hydrophobicity was performed with 50/18 cm in-house packed C18 columns (1.9 µm C18 beads, Dr. Maisch GmbH). Peptide elution was achieved with a binary solvent system (solvent A: 0.1% formic acid; solvent B: 80% acetonitrile, 0.1% formic

acid) by increasing the relative amount of B from 10 % to 38 % in a linear gradient within 35/20 min, followed by 5/3 min up to 60 % and another 5/2 min to 95%. Re-equilibration was done within 5 min at 5 %. The samples were transferred to an in line coupled QExactive orbitrap/QExactive HF mass spectrometer (Thermo Fisher Scientific) using a nano electrospray ionization source. Full MS spectra were acquired with a data-dependent Top10/15 method that comprised a resolution of 70,000/60,000 at 200 m/z and an automatic gain control (AGC) target of 3e6 at a maximum injection time of 20 ms. The 10/15 most intense ions were further fragmented with higher-energy collisional dissociation (HCD) at a normalized collision energy of 25/27 and MS² spectra were generated at 35,000/30,000 resolution, AGC target of 5e5/1e5 and maximum injection time 120/64 ms.

Data from two biological replicates (2 × 28 raw files of IgG control and anti-Flag-SINTBAD) were analyzed using MaxQuant (v1.5.5.18) (Cox and Mann, 2008) and the implemented Andromeda search engine (Cox et al., 2011). Protein assignment was accomplished with correlation of fragment spectra with the UniProt human database (July 2016). Common contaminants were excluded from the analysis. Data processing was performed with tryptic specifications and default settings for mass tolerance in MS and MS/MS spectra. The minimal peptide length was set to 7 amino acids by default and the false discovery rate on protein and peptide level was set to 1 %. Prior to further processing of the data, contaminants, reverse entries and proteins that were only identified by a modification site were filtered out. In order to define high confidence interactors, identified proteins were classified according to criteria given in suppl. Fig. 8A. Proteins from all three groups were combined and constitute the SINTBAD interactome.

Bioinformatic analysis

The volcano plots for proteins of group 2a are displayed in suppl. Fig. S13 and were done using the Instant Clue program (Version 0.5.2) (Nolte et al., 2018). The SINTBAD interactome was analysed by the STRING database version 11.0. Only interactions with a medium confidence score of 0.4 were shown. Line thickness indicates the strength of data support. The assignment of SINTBAD interactors to biological functions and processes was done by combined Genecards, Uniprot and Pubmed searches (www.genecards.org; www.uniprot.org; www.ncbi.nlm.nih.gov/pubmed). The intrinsic disorder was analyzed using the PONDR prediction tool (<http://www.pondr.com>) (Peng et al., 2005) and Espritz (Walsh et al., 2012).

Supplemental References

- Chan,E.Y., Longatti,A., McKnight,N.C., and Tooze,S.A. (2009). Kinase-inactivated ULK proteins inhibit autophagy via their conserved C-terminal domains using an Atg13-independent mechanism. *Mol. Cell Biol.* 29, 157-171.
- Chariot,A., Leonardi,A., Muller,J., Bonif,M., Brown,K., and Siebenlist,U. (2002). Association of the adaptor TANK with the I kappa B kinase (IKK) regulator NEMO connects IKK complexes with IKK epsilon and TBK1 kinases. *J. Biol. Chem.* 277, 37029-37036.
- Choi,Y., Park,S.J., Sun,Y., Yoo,J.S., Pudupakam,R.S., Foo,S.S., Shin,W.J., Chen,S.B., Tsihchlis,P.N., Lee,W.J., Lee,J.S., Li,W., Brennan,B., Choi,Y.K., and Jung,J.U. (2019). Severe fever with thrombocytopenia syndrome phlebovirus non-structural protein activates TPL2 signalling pathway for viral immunopathogenesis. *Nat. Microbiol.*
- Cox,J. and Mann,M. (2008). MaxQuant enables high peptide identification rates, individualized p.p.b.-range mass accuracies and proteome-wide protein quantification. *Nat. Biotechnol.* 26, 1367-1372.
- Cox,J., Neuhauser,N., Michalski,A., Scheltema,R.A., Olsen,J.V., and Mann,M. (2011). Andromeda: a peptide search engine integrated into the MaxQuant environment. *J. Proteome Res.* 10, 1794-1805.
- Hwang,C.Y., Holl,J., Rajan,D., Lee,Y., Kim,S., Um,M., Kwon,K.S., and Song,B. (2010). Hsp70 interacts with the retroviral restriction factor TRIM5alpha and assists the folding of TRIM5alpha. *J. Biol. Chem.* 285, 7827-7837.
- Joachim,J., Jefferies,H.B., Razi,M., Frith,D., Snijders,A.P., Chakravarty,P., Judith,D., and Tooze,S.A. (2015). Activation of ULK Kinase and Autophagy by GABARAP Trafficking from the Centrosome Is Regulated by WAC and GM130. *Mol. Cell* 60, 899-913.
- Mao,X., Gluck,N., Li,D., Maine,G.N., Li,H., Zaidi,I.W., Repaka,A., Mayo,M.W., and Burstein,E. (2009). GCN5 is a required cofactor for a ubiquitin ligase that targets NF-kappaB/RelA. *Genes Dev.* 23, 849-861.
- Nazio,F., Strappazon,F., Antonioli,M., Bielli,P., Cianfanelli,V., Bordi,M., Gretzmeier,C., Dengjel,J., Piacentini,M., Fimia,G.M., and Cecconi,F. (2013). mTOR inhibits autophagy by controlling ULK1 ubiquitylation, self-association and function through AMBRA1 and TRAF6. *Nat. Cell Biol.* 15, 406-416.
- Nolte,H., MacVicar,T.D., Tellkamp,F., and Kruger,M. (2018). Instant Clue: A Software Suite for Interactive Data Visualization and Analysis. *Sci. Rep.* 8, 12648.
- Peng,K., Vucetic,S., Radivojac,P., Brown,C.J., Dunker,A.K., and Obradovic,Z. (2005). Optimizing long intrinsic disorder predictors with protein evolutionary information. *J. Bioinform. Comput. Biol.* 3, 35-60.
- Ran,F.A., Hsu,P.D., Wright,J., Agarwala,V., Scott,D.A., and Zhang,F. (2013). Genome engineering using the CRISPR-Cas9 system. *Nat. Protoc.* 8, 2281-2308.
- Rappsilber,J., Ishihama,Y., and Mann,M. (2003). Stop and go extraction tips for matrix-assisted laser desorption/ionization, nanoelectrospray, and LC/MS sample pretreatment in proteomics. *Anal. Chem.* 75, 663-670.

Saul,V.V., Niedenthal,R., Pich,A., Weber,F., and Schmitz,M.L. (2015). SUMO modification of TBK1 at the adaptor-binding C-terminal coiled-coil domain contributes to its antiviral activity. *Biochim. Biophys. Acta* 1853, 136-143.

Seibert,M., Krüger,M., Watson,N.A., Sen,O., Daum,J.R., Slotman,J.A., Braun,T., Houtsmuller,A.B., Gorbisky,G.J., Jacob,R., Kracht,M., Higgins,J.M.G., and Schmitz,M.L. (2019). CDK1-mediated phosphorylation at H2B serine 6 is required for mitotic chromosome segregation. *J. Cell Biol.*

Tanase,C.A. (2010). Histidine domain-protein tyrosine phosphatase interacts with Grb2 and GrpL. *PLoS. One.* 5, e14339.

Van,H.S., Delaei,F., Heyninck,K., De,V.D., and Beyaert,R. (2001). Identification of a novel A20-binding inhibitor of nuclear factor-kappa B activation termed ABIN-2. *J. Biol. Chem.* 276, 30216-30223.

Walsh,I., Martin,A.J., Di,D.T., and Tosatto,S.C. (2012). ESpritz: accurate and fast prediction of protein disorder. *Bioinformatics.* 28, 503-509.